치의과학박사 학위논문

Development of Autonomous Robot Osteotomy for Mandibular Ramal Bone Harvest and Evaluation of its Accuracy

로봇을 이용한 자율적 하악골채취 골절단술의 기초방법 개발과 그 정확도 평가

2019 년 2 월

서울대학교 대학원

치의과학과 구강악안면외과학 전공

권 익 재

Abstract

Development of Autonomous Robot Osteotomy for Mandibular Ramal Bone Harvest and Evaluation of its Accuracy

Ik-Jae KWON, B.S., D.D.S.

Major in Oral and Maxillofacial Surgery

Department of Dentistry

Graduate School, Seoul National University

(Directed by Prof. Soung Min Kim, D.D.S., M.S.D., Ph.D.

and Prof. Soon Jung Hwang, Dr. med. Dr. med.dent.)

***Objectives*:** An autonomous robot osteotomy system using direct coordinate determination was developed in our study. The registration accuracy was evaluated by measuring the fiducial localization error (FLE) and target registration error (TRE) and the accuracy of the designed osteotomy method along a preprogrammed plan was evaluated. Furthermore, the accuracy of the robotic osteotomy and a manual osteotomy was compared in regard to cut position, length, angle and depth.

***Methods*:** A light-weight-robot was used in this study, with an electric gripper. A direct coordinate determination method, using three points on the teeth, was developed for registration and determination of FLE and TRE, as measured on a mandible model. Sixteen landmarks on the mandible were prepared with holes and zirconia beads and the TRE was computed in ten repeated measurements using the robot. A direct coordinate determination via three points was used for registering and a twenty stone model (7 cm x 7 cm x 3 cm). The osteotomy line was designed similar to the ramal bone graft (2 cm x 1 cm x 0.5 cm). To evaluate accuracy, we measured a position (how accurate the robot arm is located), length (how accurate the robot arm is moving while cutting), angle (the angle at which the robot arm is located), and depth (the depth of the disc cutting) error. Sixteen mandible phantoms were used to simulate the osteotomy for the ramus bone graft. An image of the phantom was obtained by three-dimensional camera scanning and a virtual ramal bone graft was designed with computer software. To evaluate an accuracy and precision, the mandible phantoms were scanned with cone beam computer tomography (CBCT). Cut position, length, angle and depth errors were measured and the results of the robotic surgery were compared with that of manual surgery.

***Results*:** The mean value of the FLE was 0.84 ± 0.38 mm and the third reference point which detected the lingual fossa of the right second molar had a larger error than the other reference points. The mean value of the TRE was 1.69 ± 0.82 mm and there were significant differences between the anterior body, posterior body,

and coronoid/condyle groups. Landmarks at the anterior body had the lowest TRE (0.96 ± 0.47 mm) and landmarks on the coronoid and condyle had the highest TRE (2.12 ± 0.99 mm). An autonomous robot osteotomy with a direct coordinate determination using three points was successfully achieved. On the model RBG osteotomy, the posterior cut had 0.77±0.32 absolute mean value, the anterior cut had 0.82±0.43, the inferior cut had 0.76 ± 0.38 and the superior cut had 1.37 ± 0.83, respectively. The absolute mean values for osteotomy errors for position, length, angle, and depth were 0.93 ± 0.45 mm, 0.81 ± 0.34 mm, 1.26 ± 1.35°, and 1.19 ± 0.73 mm, respectively. The position and length errors were significantly lower than angle and depth errors. In the comparison between robotic surgery and manual surgery, there were significant differences of absolute mean value and variance in all categories. For the robotic surgery, the cut position, length, angle and depth errors were 0.70 ± 0.34 mm, 0.35 ± 0.19 mm, 1.32 ± 0.96° and 0.59 ± 0.46 mm, respectively. For the manual surgery, the cut position, length, angle and depth errors were 1.83 ± 0.65 mm, 0.62 ± 0.37 mm, 5.96 ± 3.47° and 0.40 ± 0.31 mm, respectively. The robotic surgery had significantly higher accuracy and lower variance for cut position, length and angle errors. On the other hand, the depth error had a significantly higher absolute mean value and variance than the robotic surgery.

***Conclusions*:** An autonomous robot osteotomy scheme was developed, using the direct coordinate determination by three points on the teeth, and proved an accurate method for registration. The incisal edge or buccal pit of the teeth were

more proper reference points than the fossa of the teeth. The measured RMS of the TRE increased when the target moved away from the reference points. Robotic surgery showed high accuracy and precision in positioning and reduced accuracy in controlling the depth of disc sawing. The robotic surgery showed high accuracy and precision in positioning and somewhat low accuracy in controlling the depth of the disc sawing. Comparing robotic and manual surgeries, the robotic surgery was superior in accuracy and precision in position, length and angle. However, the manual surgery had higher accuracy and precision in depth.

Keywords: Robotics**,** Three-points coordinate determination, Robot arm, Autonomous robot, Mandibular osteotomy, Ramal bone graft

Student Number: 2014-30712

Contents

Development of Autonomous Robot Osteotomy for Mandibular Ramal Bone Harvest and Evaluation of its Accuracy

Ik-Jae KWON, B.S., D.D.S.

Major in Oral and Maxillofacial Surgery

Department of Dentistry

Graduate School, Seoul National University

(Directed by Prof. Soung Min Kim, D.D.S., M.S.D., Ph.D.

and Prof. Soon Jung Hwang, Dr. med. Dr. med.dent.)

1. Introduction

Medical robotics has tremendous potential for improving accuracy and precision when performing surgical procedures. In recent decades, medical robots have helped doctors in the operating room by doing tasks difficult to perform with human eyes and hands, and are developing rapidly. Depending on the degree of user

interaction, three categories of robot systems are defined: direct or manual control, shared control, and supervisory control robotic systems.[1] In direct control, the surgeon operates the slave robot directly through the master console. In shared control, the surgeon and controller share the manipulator command and work together in order to carry out a task. In supervisory control, the procedure is executed solely by the robot, which acts according to a computer program that the surgeon inputs prior to the procedure. In the other classification, two system groups can be distinguished in the field of surgical robotics.[2] The first group, telemanipulators, is not preprogrammed and moving exactly as controlled by a slave console. Within the other group, preprogrammed surgical robots execute a preoperatively defined trajectory.[2]

For robotic surgery, a registration process between the patient and the image should be required. The first step in a registration technique is to construct a frame-based stereotactic system.[3] The stereotactic frame should allow for rigid and exact positioning of the head and must prove itself to be very accurate and reliable.[3] Although this technique is still in use in neurosurgery, the frame is rigid and invasively fixed to the head, making it difficult to use in oral and maxillofacial surgery, because it acts as an obstacle to approaching the oral cavity. From the 1980s, with emerging computer technology frameless stereotactic systems were realized.[4] The frameless stereotactic technique includes markless pair-point registration, marker-based pair-point registration, and surface registration.[5] The reference anatomy structures can be both soft tissue and hard tissue. The use of soft tissues for reference makes it difficult to obtain accurate values because there

are many displacements, such as twisting or swelling during the operation. On the other hand, the use of bones and teeth, the representative structures for hard tissue, increases accuracy. In jaw surgery, since the operation site is defined around the teeth, registration can be most easily performed using the teeth as a reference point. Because the teeth have different aspects than bones and teeth are characterized by edges, pits, and fossae that can be touched by the probe accurately and reproducibly. Because of these special structures of teeth, accurate registration in oral and maxillofacial surgery can be obtained by using a markless technique.

In other medical fields such as orthopedic medicine, which is a field that involves hard tissue surgery, registration is accomplished by using bony anatomic structures as references.[6] However, in the case of bones, obtaining a high registration accuracy is a significant challenge because there are few definite anatomical structures that can be touched repeatedly by a probe.[7] In this scenario, increasing the number of reference points or combining different surface registration techniques can be used to reduce registration error. In contrast, in oral and maxillofacial surgery, a registration method that does not use a marker was used in this study because a tooth, which is a special case of hard tissue, can be used as a very good reference point. Because there is no need for a marker, there is no need to attach additional devices to a patient when performing preoperative computer tomography (CT). Moreover, there is no disturbance of the surgeon's vision or approach during surgery if markers are not used.

First-generation surgical robots consisted mainly of robotic arms designed to assist the primary surgeon by holding and positioning instruments such as a laparoscopic camera or retractor. Surgical robots have transcended the role of assistant to become the primary surgeon's hands through a computer interface.[8] The representative model, da Vinci Surgical System (Intuitive Surgical, Inc., Sunnyvale, CA), incorporates three-dimensional (3D) stereoscopic vision with two or three robotic slave arms equipped with instruments that have six degrees of freedom and wrist-like motions.

The direct control robots, which are represented by da Vinci, were controlled manually while viewing the screen directly by the operator, so the robots do not need to automatically determine the position of the patient. However, in the autonomous robot, the robot determines the patient coordinates, and the operation is performed based on these coordinates. Therefore, how to effectively register the patient's coordinates is an important issue for autonomous robots.

Because osteotomy is the most commonly used technique for various operations in oral and maxillofacial surgery,[9] the osteotomy design was selected for our study design. Among the many osteotomies, osteotomy for ramal bone graft (RBG) is relatively difficult to approach with good visibility. Moreover, osteotomy for ramal bone graft includes cutting in various directions using various instruments.[10] Long bone osteotomy, such as for a fibula free flap or Le Fort I osteotomy have better accessibility for the robot than the osteotomy for ramal bone graft, and are simple one-direction osteotomy examples.[11,12] Therefore, we were able to evaluate osteotomy accuracy in various directions and categories.

Conventional navigation systems are known to be relatively accurate optical tracking systems. However, optical tracking presents some inconveniences and limitations in clinical applications. A conventional optical tracking system needs a device for registering, which is bulky and can interfere with actions during an operation.[13] In addition, if several errors are accumulated due to the necessity of connecting the devices at various stages, this can result in quite large errors in the operation. By comparison, the robot arm has many advantages in accurately recognizing the required position.

Autonomous robots have several advantages over traditional navigation systems. Direct coordinate determination can be achieved by positioning that uses the physically connected robotic arm. If the robot arm can be manipulated manually and placed in a reproducibly precise position and can determine the coordinates correctly, then it can be used to register the patient's image to the operating site. In the direct coordinate determination process, at least three ordered points, which are not in one line are needed to decide the one coordinate. Theoretically, the more points that are registered, the more accurately the coordinates can be determined, but in a narrow space, such as the oral cavity, it is difficult to register multiple points and, in practice, accuracy does not increase with the addition of more points.[5] Therefore, in this study, a coordinate determination system which can be recognized by physically taking three points is suggested and applied to a robotic arm. This system we designed does not need a bulky device, such as a navigation system. In addition, if the robot can obtain high accuracy by taking only three points, the total operation time can be reduced

by shortened registration time. In this study, the registration process was conducted using only three points (direct coordinate determination by three points on the teeth) and its accuracy was evaluated. Our robot arm could detect its position and joint angle accurately within 0.1 mm. In this study, the robotic arm held the instrument and directly touched reproducible points on the model for registration.

Autogenous bone harvesting from the mandibular ramus is the first choice for reconstruction of maxillofacial defects. The mandibular ramal area has many advantages over other donor sites in the oral cavity.[10] Although the incidence of donor site complications is rare in ramal bone grafts, clinicians have made efforts to reduce potential side effects. Side effects include sensory disturbances or mandibular fractures, and can lead to unnecessary patient suffering as well as significant stress for the operating surgeons. The use of robots in an osteotomy of a ramal bone graft could lead to a more accurate osteotomy and less complications, resulting in greater patient and surgeon satisfaction. However, currently, there are no commercially available robots in the field of oral and maxillofacial surgery, and there are not many ongoing studies. Autonomous robots have not yet been developed to cut the jaw bone with burs or saws.

Because osteotomy is the most commonly used technique for many types of operations in oral and maxillofacial surgery,[9] this osteotomy design was selected for our study. Among the many types of osteotomy, osteotomy for ramal bone graft is relatively difficult to approach and the surgeon's visibility is often poor. Also, osteotomy for ramal bone graft includes cutting in various directions using various

instruments.[10] In contrast, long bone osteotomy such as for the fibula free flap or Le Fort I osteotomies has better accessibility for a robot than the osteotomy for ramal bone graft and cuts are simply in one direction.[11,12]

Various instruments such as rotary motor, laser[14], and waterjet[15] can be used during jaw osteotomy. Among these, the basic tools commonly used include a rotary motor with bur or saw. There are various burr types including: round burrs, diamond burrs, and fissure burrs. Also, there are various types of saws, such as reciprocating and oscillating. In this study, osteotomy was performed with a fissure bur or disc saw, because of the advantage gained by using these tools.

It is not easy to compare an osteotomy performed by a robot and one performed manually. Most previous studies compared robotic and manual surgeries using only qualitative methods or with indirect outcomes such as operative time.[14,16] However, these methods do not fully capture the important outcomes of the surgery.

An autonomous robot osteotomy system using direct coordinate determination was developed in our study. The registration accuracy was evaluated by measuring the fiducial localization error (FLE) and target registration error (TRE) and the accuracy of the designed osteotomy along a preprogrammed plan was evaluated. In addition, we compared the position, length, angle and depth of the cuts in the two osteotomies.

1.1. Literature review of medical robots

Medical robotics is a relatively young field, with the first recorded medical application of a robot occurring in 1985.[17] In that paper, the robot was a simple positioning device to orient a needle for biopsy of the brain. Research groups in Europe, Asia, and the United States began investigating medical applications of robotics: In Europe, a group at Imperial College in London under the direction of Davies began developing a robot for prostate applications,[18] at Grenoble University Hospital in France, Benabid and colleagues started work on neurosurgical applications such as biopsy,[19] in Asia, Dohi and colleagues at Tokyo University developed a prototype of a computed tomography (CT)-guided needle insertion manipulator,[20] and in the United States, Taylor and associates at IBM began developing the system later known as ROBODOC.[21] Currently, there are several commercial ventures and a handful of research laboratories active in the field of medical robotics. Clinical applications are more interesting to the end-user, and a list of seven clinical areas where robotics have been applied appears, such as the fields of neurosurgery, orthopedic, urology, maxillofacial, radiosurgery, ophthalmology, cardiac.[22]

First-generation surgical robots consisted mainly of robotic arms designed to assist the primary surgeon by holding and positioning instruments such as a laparoscopic camera or retractor. Surgical robots have transcended the role of assistant to become the primary surgeon's hands through a computer interface.[8] The representative model, da Vinci Surgical System (Intuitive Surgical, Inc.,

Sunnyvale, CA), incorporates three-dimensional (3D) stereoscopic vision with two or three robotic slave arms equipped with instruments that have six degrees of freedom and wrist-like motions.

Preprogrammed surgical robot is the other type of robot system that is distinct from da Vinci system. The robot is given autonomy and moves according to the preoperative surgical plan designed on the computer. Weihe et al. evaluated the practicability of intraoperative instrument navigation and robotics that performs osteotomy of the temporal bone designed in the computer system based on the original CT data set at the animal model.[23] In the other area, Majdani et al introduced a robot-guided minimally invasive approach for cochlear implant.[24] In the field of radiation treatment, robotic assistance for fully automated brachytherapy seed placement into skull base was studied.[25] The performance of robot-assisted skull base brachytherapy was feasible and accurate. Another example is robot-guided stereoelectroencephalography (SEEG) that has demonstrated comparable operative efficiency, accuracy, and safety as well as epilepsy outcomes compared to previously published robot-guided and nonrobot-guided SEEG series.[26]

In the medical field, robots have been helping people directly or indirectly for a long time. Teleoperative robots are already used in many areas of oral and maxillofacial surgery, for example cancer surgery,[27,28] reconstructive surgery,[29,30] and benign tumor resection.[31] For reconstructive surgery, Katz et al. demonstrated that the da Vinci robot can be used to successfully perform vessel micro-anastomoses in a porcine model.[29] In addition, robot-assisted surgeries in both

phantom and animal models were performed for mandibular fibula free flap reconstruction.[30] One of the most actively studied techniques in robotic maxillofacial surgery is tumor surgery. For example, some surgeons are developing robot-assisted neck dissection for the treatment of head and neck cancer.[27,28] In addition, robot-assisted submandibular gland excision via modified facelift incision has been performed.[31]

Telescopic surgery using the master-slave console has come a long way, but autonomous robots for clinical applications have been relatively slow to develop. In an autonomous robotic study in the field of reconstructive surgery, pre-programmed robotic osteotomies for free fibula flap mandible reconstruction were performed using an autonomous robot arm.[32] In the field of orthognathic surgery, robots are being used for various purposes, from using a robotic arm for Le Fort I osteotomy[12] to repositioning the maxilla using an autonomous robot arm.[33] In addition, some researchers perform a mandibular angle split osteotomy using specialized robot-assisted arms.[34] Autonomous robots have also been applied in the dentoalveolar field to accurately hold the maxillofacial implant in position.[35] The robot holds the drill handpiece and moves only when the surgeon applies manual pressure to the drill handpiece. The robot leads the surgeon to the preoperatively planned implant position and permits handpiece movement only along the selected drilling axis. In addition, an animal experiment using a robot arm was performed for an osteotomy using a laser.[16]

Maxillofacial surgery is a branch of surgery that is concerned primarily with operations on the jaws and surrounding soft tissues. In many maxillofacial surgical

cases, it is necessary to manipulate the bone by drilling, cutting, shaping and repositioning. Accuracy is at a premium, because the shape of the bone and the esthetic appearance of the skull and face are extremely important to patients. As robots can often achieve exquisite accuracy with bone, maxillofacial surgery is a promising application area for robotics.[36] Moreover, 3D-simulation technology with haptic feedback may improve the care of oral and maxillofacial surgical patients. These innovations are improving the scope of telemedicine and have the potential to advance a variety of options for treating oral and maxillofacial trauma and reconstruction.[37]

2. Materials and Methods

2.1. Robotic System

A light-weight-robot (KUKA LBR iiwa 7 R800, KUKA Robotics, Augsberg, Germany) was used to position the gripper and dental handpiece. This robot features seven degrees of freedom and provides an adjustable range of movement up to either 170° or 120°. The robot is extremely sensitive because of its integrated sensors, which make it ideal for force-controlled tasks. The robot arm is a precise, lightweight robot for delicate assembly work. It has seven axes for maximum versatility, a 7 kg rated payload, and 800 mm of maximum reach. In all seven axes, the robot has joint torque sensors, implemented using a safe and proven technology.

We used an electric 2-finger parallel gripper (SCHUNK GmbH & Co. KG, Germany) and designed the flange of the robot arm with the finger of the gripper (Figure 1a). The dental handpiece with a fissure bur was tightly held by the gripper and it acted as a registration probe (Figure 1b).

2.2. Overview of System

The robot consisted of four parts (Figure 1c):

(a) Workbench notebook

(b) Robot controller (cabinet)

(c) Robot arm

(d) SmartPAD®

An application was programmed using the workbench notebook. After uploading the program to the robot controller, we ran the application on the robot arm. It was possible to operate the robot through the smartPAD®, and the robot could be operated manually by the smartPAD® or automatically by the preprogrammed application.

A gripper was connected to the end of the robot arm, and this gripper held a dental low-speed handpiece connecting a disc saw or fissure bur for bone cuttingas shown Figure 2. We used two different tools with a surgical fissure bur (2-mm diameter and 15-mm length cutting edge) and two kinds of discs (6-mm and 20-mm diameter with 0.5-mm thickness).

2.3. Three-Point Coordinate Determination

In most robot systems involving motion, registration of preoperative 3D imaging and the actual patient or model is required. Our robot arm could detect its position and joint angle accurately within 0.1 mm. In this study, the robotic arm held the instrument and directly touched three reproducible points on the teeth of the mandible model to achieve registration.

The robot uses a Cartesian coordinate system and Euler angles to indicate the position, with the parameters X, Y, Z, α, β, and γ. The values of X, Y, and Z are

the amounts of translation along the x-, y-, and z-axes, respectively. The radians of α, β, and γ are the values of the Euler angles rotated with respect to the z-, y-, and x-axes, respectively. The Euler angles are three angles introduced by Leonhard Euler to describe the orientation of a rigid body with respect to a fixed coordinate system.[38] By using three elemental rotations, any orientation can be achieved.

The Euler angle conversion method considers three rotations with respect to one of three axes three times, in which the order of rotations is very important. As shown in Figure 3a, when the i-coordinate system and the m-coordinate system, having an arbitrary three degrees of freedom coordinate transformation relation, rotations in the following must be applied in order to match the base vectors of both coordinate systems relative to the specified axis.

1) Rotation by α radians with respect to the z-axis (or K_i-axis)

2) Rotation by β radians with respect to the y-axis (or J_1-axis)

3) Rotation by γ radians with respect to the x-axis (or I_m-axis)

When we refer to the order of the unit coordinate transformations, the complex coordinate transformation matrix from the i-coordinate system to the m-coordinate system can be seen as follows.

$$C_i^m = C_2^m C_1^2 C_i^1$$

$$C_2^m = C_x(\gamma) = \begin{pmatrix} 1 & 0 & 0 \\ 0 & cos\gamma & sin\gamma \\ 0 & -sin\gamma & cos\gamma \end{pmatrix}$$

$$C_1^2 = C_y(\beta) = \begin{pmatrix} cos\beta & 0 & -sin\beta \\ 0 & 1 & 0 \\ sin\beta & 0 & cos\beta \end{pmatrix}$$

$$C_2^m = C_z(\alpha) = \begin{pmatrix} cos\alpha & sin\alpha & 0 \\ -sin\alpha & cos\alpha & 0 \\ 0 & 0 & 1 \end{pmatrix} \quad (1)$$

Therefore, by multiplying each matrix of equation (1) and summarizing the results, it can be seen that the complex coordinate transformation matrix from the i-coordinate system to the m-coordinate system is constructed as follows.

$$C_i^m = \begin{pmatrix} cos\beta cos\alpha & cos\beta sin\alpha & -sin\beta \\ sin\gamma sin\beta cos\alpha - cos\gamma sin\alpha & sin\gamma sin\beta sin\alpha + cos\gamma cos\alpha & sin\gamma cos\beta \\ cos\gamma sin\beta cos\alpha + sin\gamma sin\alpha & cos\gamma sin\beta sin\alpha - sin\gamma cos\alpha & cos\gamma cos\beta \end{pmatrix} \quad (2)$$

Conversely, when a coordinate transformation from the m-coordinate system to the i-coordinate system is required, the following relational expressions are used.

$$C_m^i = (C_i^m)^T = \left(C_i^1\right)^T (C_1^2)^T (C_2^m)^T$$

$$\left(C_i^1\right)^T = C_z(-\alpha) = \begin{pmatrix} cos\alpha & -sin\alpha & 0 \\ sin\alpha & cos\alpha & 0 \\ 0 & 0 & 1 \end{pmatrix}$$

$$(C_1^2)^T = C_y(-\beta) = \begin{pmatrix} cos\beta & 0 & sin\beta \\ 0 & 1 & 0 \\ -sin\beta & 0 & cos\beta \end{pmatrix}$$

$$(C_2^m)^T = C_x(\gamma) = \begin{pmatrix} 1 & 0 & 0 \\ 0 & cos\gamma & -sin\gamma \\ 0 & sin\gamma & cos\gamma \end{pmatrix} \quad (3)$$

$$C_m^i = \begin{pmatrix} cos\beta cos\alpha & sin\gamma sin\beta cos\alpha - cos\gamma sin\alpha & cos\gamma sin\beta cos\alpha + sin\gamma sin\alpha \\ cos\beta sin\alpha & sin\gamma sin\beta sin\alpha + cos\gamma cos\alpha & cos\gamma sin\beta sin\alpha - sin\gamma cos\alpha \\ -sin\beta & sin\gamma cos\beta & cos\gamma cos\beta \end{pmatrix} \quad (4)$$

Likewise, equation (4) shows the complex coordinate transformation matrix from the i-coordinate system to the m-coordinate system.

One Cartesian coordinate system can be determined by three different points in space that are not on the same line. We used a robot arm holding the instrument to detect three points in space and used these 3D positioning values to calculate

the new Cartesian coordinate system to match the preoperative image and actual position.

In Figure 3b, the overview of direct coordinate determination by three points on the teeth is represented. When each three reference points were detected, the robot calculated the model coordination step by step. The first point represents the origin of the new coordinate. The second point is used for determining the x axis. The direction from the first point to the second point is in the positive x-axis direction. Finally, the third point is first used for determining the xy-plane. The z axis is then defined as an axis passing through the origin perpendicular to the xy-plane and calculated by the cross product of x vector and y' vector, which starts at the first point, and proceeds in the direction of the third point. The y axis is defined automatically by the z and y axis and is calculated by their cross product.

In the robot world coordinate system, the axis vectors such as $\begin{pmatrix} |\vec{x}| \\ 0 \\ 0 \end{pmatrix}$, $\begin{pmatrix} 0 \\ |\vec{y}| \\ 0 \end{pmatrix}$, and $\begin{pmatrix} 0 \\ 0 \\ |\vec{z}| \end{pmatrix}$ are transformed to the vectors of $\begin{pmatrix} x_1 \\ x_2 \\ x_3 \end{pmatrix}$, $\begin{pmatrix} y_1 \\ y_2 \\ y_3 \end{pmatrix}$ and $\begin{pmatrix} z_1 \\ z_2 \\ z_3 \end{pmatrix}$ in the model coordinate system, respectively.

Now that the following equations (5) are determined, we can calculate the values of α, β, and γ using equation (4).

$$C_{world}^{model} \begin{pmatrix} |\vec{x}| & 0 & 0 \\ 0 & |\vec{y}| & 0 \\ 0 & 0 & |\vec{z}| \end{pmatrix} = \begin{pmatrix} x_1 & y_1 & z_1 \\ x_2 & y_2 & z_2 \\ x_3 & y_3 & z_3 \end{pmatrix} \quad (5)$$

As a result, the values of α, β, and γ can represent the position of the robot arm according to the model coordinate system.

2.4. Evaluation of Registration Accuracy

2.4.1. Study Design

Ten in-vitro registrations were performed on a mandible phantom (Pacific Research Laboratories Inc., Vashon, WA, USA) using direct coordinate determination by three points on the teeth. The distal edge of the mandibular left lateral incisor, the buccal pit of the left second molar, and the lingual fossa of the right second molar were chosen as the three points for this registration system. The robot arm recognized the position of the three points by directly touching them manually.

The mandible model was prepared with landmarks. The landmarks were created by drilling 1 mm holes in the model. A drilling diameter of 1 mm was selected in order for the holes to be clearly visible using cone beam computer tomography (CBCT). A total of sixteen landmarks were spread over the mandible. Four landmarks were placed on the anterior chin area, and a total of eight landmarks were placed on both posterior ramus areas on either side. Additionally, a total four landmarks were placed on the coronoid process and condyle head on both sides of the mandible. For each landmark, a 1 mm diameter zirconia sphere bead was put in the hole so it could be clearly determined on the CBCT image. At the selected three reference points on the teeth, zirconia beads were also placed for visibility (Figure 4).

The mandible model was scanned using CBCT (Point 3D Combi 500, Pointnix Inc., Seoul, Korea). All landmarks were manually identified on the coronary, sagittal, and axial slices, as well as on the three-dimensional surface (Figure 5).

2.4.2. Accuracy Evaluation

In pair-point registration, the fiducial localization error (FLE) denotes the error that occurs when points in the image data or on the model are marked for registration. The true reference values of the x, y, z coordinates of the three reference points were measured from the CBCT data using 3D software (MIMICS 19.0, Materialise, Leuven, Belgium). The coordinates of each of the three points were measured ten times using a robot arm gripping a sharp pointer by touching the points that were compared with the true value to measure the FLE. The FLE values with respect to the x-, y-, z-axes were calculated by differences between the measured data and true data. Absolute mean values of $\Delta x, \Delta y, \Delta z$ and the root mean square (RMS, $\sqrt{\Delta x^2 + \Delta y^2 + \Delta z^2}$) were calculated to evaluate the fiducial marker accuracy

After finishing the registration, the mandible model coordination could be defined and the target landmarks could be read in model coordination. All sixteen landmarks in the mandible were targeted using a robot arm gripping the sharp pointer and this process was repeated ten times. The robot calculated the x, y, z coordinates of the pointer based on the model coordination. The target registration errors (TRE) by x-, y-, z-axes were calculated by differences between the measured data and true data. Absolute mean values and the RMS

($\sqrt{\Delta x^2 + \Delta y^2 + \Delta z^2}$) were calculated to evaluate the target accuracy. For each of the sixteen landmarks, the ten measurements of the TRE were averaged. The examined landmarks were categorized into the left and right side and also categorized into the anterior chin area, posterior ramus area, and the coronoid/condyle.

Statistical analysis was performed using the statistical package for the social sciences (SPSS for Windows releases 21.0.0.0, SPSS Inc., Chicago, IL, USA). The descriptive statistics for the FLE and TRE were presented in terms of an absolute mean ± standard deviation (SD). T-tests and one-way ANOVA with post-hoc (Tukey's) were used for comparison of the categories.

2.5. Autonomous Robot Osteotomy and its Accuracy evaluation

2.5.1. Study Design

Twenty rectangular stone models (7 cm x 7 cm x 3 cm) were designed for the test bench. To use direct coordinate determination by three points, we touched the three different points on the upper plane of the model by hand manipulating the robot arm gripping the pointer. The robot was set on impedance mode, which modulates the joint impedance. By decreasing the joint impedance, the robot could be manipulated easily by hand. After coordinate determination, the robot arm

automatically determined the osteotomy position. The osteotomy line was designed similar to the ramal bone graft line (2 cm x 1 cm x 0.5 cm), and divided into posterior, anterior, inferior, and superior cuts. The posterior and anterior line was cut by a fissure bur. The posterior part was performed first with a 10 mm position and 5 mm length, and the anterior part was performed similarly 20 mm apart from the posterior part. Subsequently, the tool was manually changed to the disc saw to cut the inferior and superior lines. At the inferior cut, the disc saw was located anteriorly first and achieved a 5 mm depth, and then proceeded to the posterior direction with 20 mm length along a straight line. At the last superior cut, the robot arm was rotated three-dimensionally for proper positioning and cutting the 20 mm line with a 5 mm depth (Figure 6a).

2.5.2. Accuracy Evaluation

Each position, length, angle, and depth of the four cuts (posterior, anterior, inferior, and superior) were measured by an electronic caliper and goniometer. Errors of position, length, angle, and depth for accuracy evaluation of the osteotomy cutting line were considered by calculating the difference between the planned values and results. The position error was defined as the difference between the preplanned position and the actual robot arm position. The position error on the x-axis could not be measured, because the robot approached the test model and utilized its position as a reference point when it came into contact with the surface during the osteotomy procedure. So the position error could be measured on only the y- and

z-axes. The posterior cut started at the origin of the coordinate system. Length error was defined as the differences in sliding fissure bur cuts of the anterior and posterior parts from the preplanned 5 mm. Angle error was defined as the angle differences between the bur and disc within 90 degrees. Finally, depth error was defined as indicating the depth difference of inferior and superior disc cuts. The length differences were measured at two points, top and bottom. In the inferior and superior cuts, position and angle were measured at the two points, anterior and posterior, and depth was measured at the three points: anterior, middle and posterior. Absolute mean values for all error types were calculated and the RMS of the position error was obtained additionally (Figure 6b).

Statistical analysis was done using SPSS for Windows release 21.0.0.0 (SPSS Inc., Chicago, IL, USA). Descriptive statistics for errors were presented as absolute mean±standard deviation (SD). One-way ANOVA with Tukey's post-hoc was used for comparison of each error type.

2.6. Comparison of Robot and Hand RBG Osteotomy on Mandible

2.6.1. Design for 3D virtual planning

A total of sixteen mandible phantoms (Pacific Research Laboratories Inc., Vashon, WA, USA) were used to simulate ramal bone graft osteotomy. A 3D image of a

phantom was obtained by 3D scanning and a virtual ramal bone graft was performed using the MIMICS 19.0 software (Materialise, Leuven, Belgium). To perform the ramal bone graft osteotomy, the robot should know the transformation from the mandible coordinate to the ramus coordinate. A coordinate of the phantom model was determined by three-point coordinate determination. The three points could be detected easily (Figure 7a):

(1) The distal edge of the mandibular left lateral incisor

(2) The buccal pit of the left second molar

(3) The lingual fossa of the right second molar.

The ramal bone graft was designed with a virtual model with a thickness of only 0.3 cm (2 cm x 1 cm x 0.3 cm). For ramal bone graft mandible osteotomy, one more transformation was needed such as transformation from the phantom coordinate to the ramus coordinate. A two-transformation matrix was calculated from equation (4) and multiplied to obtain the final transformation matrix. After solving the equation, the final position of the robot arm (X, Y, Z, α, β and γ) based on the ramus coordinate could be obtained. Finally, the robot could detect the ramus coordinate and perform the ramal bone graft osteotomy on the preprogrammed position (Figure 7b).

On the left side, the robot surgery was performed as described above, and on the right side, a conventional manual surgery was performed in the same order as the robotic surgery. For the manual surgery, surgical instruments and measuring tools from a typical actual surgery were used in an operating room. A surgical ruler and pencil were used to design the ramal bone graft osteotomy. The osteotomy

started at the fixed reference point, which was defined as the point 29 mm from the lingual groove of the right second molar and the anterior ramus. After that, the other osteotomy line was traced so that it mirrored that on the left side (2 cm x 1 cm x 0.3 cm).

For the posterior and anterior cuts, the surgery was done with a fissure bur in hand. For a 10-mm cut, the fissure bur moved into the model 3-mm deep on both sides. For the inferior and posterior cuts, we divided the robot surgery group into two groups: 6-mm diameter disc and 20-mm diameter disc. Among the sixteen total mandible phantoms, eight were in the 6-mm disc group and eight were in the 20-mm disc group. For all sixteen phantoms, the left side was operated on by the robot and the right side was operated on manually.

2.6.2. Comparision and Evaluation

After ramal bone graft osteotomy on both ramal bones, cone beam computer tomography (CBCT; Point 3D Combi 500, Pointnix Inc., Seoul, Korea) was used to evaluate the osteotomy. The CBCT images were reconstructed to form 3D images using MIMICS software. On the software, a preplanned design was aligned to the CBCT image so we could measure the differences in position, length, angle and depth of the cuts made for the ramal bone graft osteotomies. Each position, length, angle and depth of the four kinds of cuts (posterior, anterior, inferior and superior) were measured using the 3D software.

The position error on the x-axis could not be measured because the robot approached the test model and took its position as a reference point when it came into contact with the surface during the osteotomy. Thus, the position error could only be measured on the y- and z-axes. For measuring the depth of the inferior and superior cuts, we sliced the mandible model at the position of the posterior and anterior osteotomy on the software. At these sections, we could easily measure the depth of the cut. For the inferior and superior cuts, the position and angle were measured at two points: anterior and posterior, and the depth was also measured at two points: anterior and posterior. The absolute mean values for all the errors were calculated and the root mean square (RMS) of the position error was additionally obtained. These parameters were measured on both sides using the same method (Figure 8).

Statistical analysis was performed using the statistical package SPSS for Windows (release 21.0.0.0, SPSS Inc., Chicago, IL, USA). Descriptive statistics for mean error and RMS of position, angle and length measurements are presented as the mean ± standard deviation (SD). The results of the robotic surgery group and manual surgery group were compared by t-test. A *p*-value of 0.05 or less was regarded as statistically significant.

3. Results

3.1. Flow diagram

Our autonomous robotic osteotomy system for a ramal bone graft was divided into three main actions: referencing, stone RBG osteotomy and mandible RBG osteotomy. In the referencing machine, the position values of the three reference points detected by the robot arm were gathered and the data were sent to the three-points coordinate determination machine. In the direct coordinate determination machine, x, y, z, α, β and γ for a transformation from robot coordinate to model coordinate were calculated using Euler angle transformation. Then the robot could recognize the coordinate of model, and perform the model osteotomy as preprogrammed plan. At the third machine, the mandible RBG osteotomy, one more transformation module from the mandible coordinate to the ramus coordinate was added. Thus, before doing the mandible ramal bone graft osteotomy, two Euler transformations are obtained. By combining these two transformations, the robot could determine final coordinates for the ramal bone graft osteotomy (Figure 9).

3.2. Registration Accuracy

To determine registration accuracy of direct coordinate determination by three points on the teeth, the FLE and TRE of this system were analyzed. The beads of the reference points and landmarks could all be clearly identified on the reconstructed CBCT image. Table 1 presents the results of the absolute differences in the x-, y-, and z-axes, and RMS between the positions in planning and the intraoperative detection for each of the three reference points. The RMS of the FLE was 0.84 ± 0.38 mm. The third reference point, which detected the lingual fossa of the right second molar had the largest error among the reference points (Table 1).

The TRE was analyzed at 16 landmarks on the mandible. Table 2 represents the results of absolute differences in the x-, y-, and z-axes, and the RMS between the value detected by the robot and the true value measured using the CBCT data. The overall RMS of the TRE was 1.69 ± 0.82 mm. Landmarks were categorized into the right/left sides (left group: #1-#8, right group: #9-#16) and the locations (anterior chin area group: #7, #8, #15, #16, posterior ramus area group: #3-#6, #11-#14, coronoid/condyle group: #1, #2, #9, #10). Table 3 represents the results of the absolute mean value and RMS of the TRE categorized by the right/left side and location. There was no significant difference between the left side and right side (Figure 10). Among the locations, there were significant differences between the anterior area, posterior area, and coronoid/condyle groups. Landmarks at the

anterior area had the lowest TRE (0.58 ± 0.17 mm) and landmarks at the coronoid and condyle had the highest TRE (2.12 ± 0.99 mm) (Figure 11).

3.3. Autonomous Robot Osteotomy and its Accuracy

The direct coordinate determination by three points and model RBG osteotomy were used for registration. The registration of each of twenty rectangular models was done by only three reference points using the robotic arm. After the direct coordinate determination, the robot could perform the RBG operation by itself. The robot could automatically determine the position of origin and start the RBG osteotomy at that position. The robot moved along the x-axis and stopped when it touched the model surface. When an alarm indicating that the model had been touched sounded, the handpiece motor was turned on to perform the cutting. All instruments, including the fissure bur and 20 mm disc, could be programmed identically such that when the surface was detected, the handpiece was turned on to cut the model. At first, a fissure bur was used for posterior and anterior cuts, and then the instrument was changed to the disc saw to cut inferiorly and superiorly (Figures 10).

A total of twenty models were used to test the osteotomy using a robot arm. Each error for the RBG osteotomy model is summarized in Table 4 by cut type. The absolute mean values for osteotomy errors for each cut type are represented in Table 5. The posterior cut had a 0.77 ± 0.32 mm absolute mean value, the

anterior cut had 0.82 ± 0.43 mm, the inferior cut had 0.76 ± 0.38 mm, and the superior cut had 1.37 ± 0.83 mm, respectively. The superior cut had the highest absolute mean error, but there was no significant difference (Table 5). The absolute mean values for osteotomy errors for position, length, angle, and depth were 0.93 ± 0.45 mm, 0.81 ± 0.34 mm, 1.26 ± 1.35°, and 1.19 ± 0.73 mm, respectively. The position error was estimated by the direction of the y- and z-axes, and RMS value was calculated. There was a significant difference between each group. The position error was significantly lower than the angle and depth errors. Similarly, the length error was significantly lower than the angle and depth errors (Table 6 and Figure 12).

3.4. Comparison between the Robotic and Manual Ramal Bone Graft Osteotomy on Mandible

Shown as a flow diagram in Figure 9, the transformation module was needed for mandible ramal bone graft osteotomy. The direct coordinates were determined using three points on the teeth, and these were used to register the mandible phantom model to the robot. The three reference points on the mandibular teeth included the distal edge of the mandibular left lateral incisor, the buccal pit of the left second molar and the lingual fossa of the right second molar. To reduce the registration error, these three reference points were defined as the points that could be taken with the greatest distance from each other in the oral cavity. The

order in which these were performed is depicted in Figure 7. The three points were detected in order, and then the mandible-coordinate was determined. Next, the robot calculated the transformation automatically and positioned itself at the origin of ramus-coordinate. The ramal bone graft osteotomy could start at these points using the same algorithm as was used in a previous model ramal bone graft osteotomy.

We performed a total of sixteen mandibular phantom surgeries using robotic surgery on the left side and using manual surgery on the right side with the same phantom model (Figure 13). After finishing the phantom surgeries, both osteotomy lines were compared by the naked eye. The manual surgery tended to result in irregular lines, but all the robotic surgeries resulted in straight lines.

Each category of errors for the mandible ramal bone graft osteotomy by the type of cuts is summarized in Table 7. The position error was measured by y- and z- axes and calculated as RMS values. Comparing the 6-mm disc and 20-mm disc groups, depth error was significantly higher on the 20 mm-disc group than on the 6 mm-disc group (p = 0.009) only on the superior cut of the robotic surgery (Table 7). Comparing robotic surgery and manual surgery, there were significant differences in absolute mean value and variance in all categories (Table 8). For robotic surgery, the position, length, angle and depth errors were 0.70 ± 0.34 mm, 0.35 ± 0.19 mm, 1.32 ± 0.96° and 0.59 ± 0.46 mm, respectively. For the manual surgery, the position, length, angle and depth errors were 1.83 ± 0.65 mm, 0.62 ± 0.37 mm, 5.96 ± 3.47° and 0.40 ± 0.31 mm, respectively. The robotic surgery had significantly higher accuracy and lower variance for position, length and angle

errors. On the other hand, the absolute mean value and variance of the depth error was significantly higher for the robot surgery (Table 8 and Figure 14).

3.5. Ergonomics and safety

We tested the ease with which the posterior mandibular ramal area could be approached by the robot arm osteotomy through an intraoral approach in the dummy operating theater. The surgeons' natural position could be guaranteed and enough space was provided (Figure 15). The vertical cut with the long fissure bur and the inferior cut were successfully simulated in the direct direction toward the operating site. For the superior cut, the robot arm should be rotated to horizontal. We set the midpoint of robot position so that when the robot turned, it did not hit the patient or the surgeon.

The ergonomic aspects and safety features of robot guidance were assessed and confirmed under optimal conditions. The computer-assisted, robot arm osteotomy was compact enough to allow two surgeons to operate comfortably. To ensure safety of the patient, the robot would automatically stop if the robot arm was subjected to a torque of 15 N or more. Also, the handpiece engine was only manually operated. Our robot system is equipped with an emergency button on the smartPAD® that allows the robot to stop when an unexpected event occurs.

4. Discussion

An autonomous robot osteotomy scheme was developed and it was demonstrated that direct coordinate determination by three points on the teeth was an accurate method for registering the image data. Our developed registration system was evaluated for registration errors. The value of FLE, the distance between the true and measured position of the fiducial markers, and TRE, the distance after registration between the target position in one space and its counterpart in the other space, were measured. Three points were used for registration and each FLE was measured as 0.62 ± 0.18 mm, 0.70 ± 0.34 mm and 1.21 ± 0.32 mm. The third point, the lingual fossa of the second molar had a significantly lower accuracy than the other reference points. The incisal edge of the teeth and buccal pit of the molar proved to be more proper reference points for detection by the robot arm relative to the lingual fossa of the teeth. Therefore, when determining the reference point, it is best to consider these results.

Our direct coordinate determination system used three teeth anatomical structures as markless fiducial points. The markless pair-point registration using just three points is known to have a lower accuracy than other methods.[5] However, in the oral cavity, the edge and pit of teeth could be easily and repeatedly detected by the robot arm, as such the accuracy of our markless system is higher for this application. The total absolute mean value of the TRE was 1.69 ± 0.82 mm. This result was comparable with those of other studies exploring the accuracy of

registration.[39,40] These registration errors ranged from 1.5 mm to 2.0 mm. Our results were also comparable with those for other registration methods, such as laser surface scanning, bone-implanted fiduciary markers, and the splint method.[41,42] The accuracy of our registration system depended on the geometry of the registration point configuration. At the anterior chin area, the RMS of the TRE was 0.96 ± 0.47 mm. Since the location of this target is closest to the origin, the incisal edge of lateral incisor, the smallest error occurred at this point. In contrast, in the coronoid/condyle area, the RMS of the TRE was 2.12 ± 0.99 mm, which was a significantly higher value than the errors found in other areas. The coronoid or condyle area appears to be the most distant from the reference points, resulting in the largest error. This result agrees with the conclusion of another similar study.[40]

There are several ways to register 3D patient data. The 3D image can be matched by point sets, lines, or surfaces.[43] Among these techniques, point sets can be useful for registering using only the robot arm, without additional devices. When using our direct coordinate determination by three points on the teeth, it is very important to know how accurately the robot arm can be controlled by manually detecting the points. Soft tissue points are not suitable for registration because they can be easily deformed during oral and maxillofacial surgery. However, the edge, pit, or fossa of a tooth is a proper anatomical structure which is near the surgical area and can be easily and reproducibly detected for reducing errors. In addition, it is important that the robot arm can be very easily handled and manipulated. The robot we used could adjust the impedance value for each joint,

and when it was set to a very low value, the robot arm could be easily moved by hand manipulation. In fact, using the robot, we were able to record precisely the point we wanted, such that a small error could be obtained.

The autonomous robot osteotomy was developed and the direct coordinate determination by three points was an accurate method for registration. Conventional navigation systems are known as relatively accurate optical tracking systems. However, there are some inconveniences and limitations in several applications. Conventional navigation systems should be equipped with a reference point through a device designed from the time of pre-operative CT, and a device for fixing the skull or fixing the position of the facial bone to the head during surgery. In addition, if several errors are accumulated due to the necessity of connecting the devices at various stages, quite large errors will be recognized in the operation. Lee et al. reported that the RMS differences for an optical navigation system between the planning and postoperative computed tomographic model were 1.31 ± 0.28 mm and 1.74 ± 0.73 mm, respectively.[13] In another study, the ROSA robot guidance platform using skull fiducial or laser registration had a 1.75 ± 0.94 mm radial error, 2.82 ± 1.1 mm depth error, and 3.39 ± 1.078 mm target point error.[26] In our system using direct coordinate determination, the position, length, angle, and depth errors were 0.93 ± 0.45 mm, 0.81 ± 0.34 mm, 1.26 ± 1.35°, and 1.19 ± 0.73 mm, respectively. Although the angle and depth errors were larger than the position and length errors, our system was accurate compared to autonomous robot studies using other registration methods.

For the posterior and anterior cuts, robot osteotomy was designed such that the fissure bur was sliding in the model by 5 mm as the width of ramal bone graft design. The length error represented the accuracy of this action. Moreover, for inferior and superior cuts, the 20 mm diameter disc saw moved into the model with a 5 mm depth and a slide with 20 mm length. Depth error represented the accuracy of how deep the disc moved into the model. These depth and angle errors were quite large compared with the position and length errors. The position error is position-dependent when the robot arm moves without any resistance, but the depth errors are affected by the changing resistance depending on the density of the model which corresponds to bone in an actual patient. Therefore, the depth error tended to be larger than the other errors. The control of angular deviation is a different issue from positioning the end point. Our results demonstrated that the angular control of the end effector could be more difficult than position control.

In 1991, Taylor et al. performed the first orthopedic surgery for hip replacement using the ROBODOC surgical device, which was the first system that could implement a preplanned milling trajectory.[21] In oral and maxillofacial surgery, the first application of robot-assisted surgery was by Kavanagh, who performed preclinical tests of antrostomy using the ROBODOC system.[44] In 1998, the OTTO system (Surgical Robotics Laboratory, Medical Faculty Charité, Humboldt-University, Berlin, Germany) was developed as the first interactive robotic system for positioning an electric drill in maxillofacial surgery.[36] To the best of our knowledge, no robotic system has been specifically designed for cranio-maxillofacial reconstruction, particularly in hard tissue surgery.[30] In particular,

there are no commercially available robots in the oral and maxillofacial surgery field, and there are not many ongoing studies.

Medical robotics represents one of the fastest growing sectors in the medical devices industry. We propose six levels of autonomy for medical robotics as one possible framework. Level 0: No autonomy, Level 1: Robot assistance, Level 2: Task autonomy, Level 3: Conditional autonomy, Level 4: High autonomy, and Level 5: Full autonomy.[45] Robot assistance means that the operator maintains continuous control of the system while the robot provides specific assistance and task autonomy means that the operator maintains discrete control of the system, and the robot can perform specific operator-initiated tasks automatically. Robot-assisted surgery and robot-guided surgery belongs to Level 1, Robot assistance. Our robot arm belongs to Level 2, Task autonomy, as it can partially perform tasks automatically. This study is a new attempt to use an autonomous robot in the maxillofacial region and goes one step further to a higher level of autonomy.

Mandible ramal bone graft osteotomy on a phantom model was performed successfully. There was no significant difference between the 6-mm disc group and the 20-mm disc group during both robotic and manual surgery. This means that there was no difference in the accuracy of the kinds of tools when either the robot or the person was operating. We recognized that the instrument was detecting the surface of the mandible model and made it work accordingly, so both 6-mm and 20-mm discs should work with the same program, and the accuracy with the different kinds of instruments should not be significantly different. However,

comparing the robotic and manual surgeries, there were significant differences in many categories.

The error was calculated by dividing by the mean value and the RMS. The accuracy of a measurement system is the degree of closeness of measurements of a quantity to that quantity's true value. The precision of a measurement system, related to reproducibility and repeatability, is the degree to which repeated measurements under unchanged conditions show the same results. Considering these metrics, robotic surgery was better than manual surgery for the position and length errors in both accuracy and precision. The position error is an indicator of how accurately the end effector of the robot is located and the length error is an indicator of how accurately the end effector of the robot has moved during osteotomy of the model. Thus, obviously the robot can be positioned and moved more accurately and precisely than a person’s hand. In the angle error, there was a different result. The mean value of angle error was not significantly different between robotic and manual surgery, but the RMS of the angle error was significantly different between the groups. There was no difference in accuracy between the two groups in adjusting the angles to position the instruments. In this study, only the angle of 90° was used for the osteotomy design. The 90° angle can be measured relatively accurately by the human naked eye. Therefore, there seems to be no difference in accuracy between the two groups. If we designed it at an arbitrary angle, such as 30°, 45° or 60° rather than 90°, the results might have been different. In regard to precision, the robot was better than humans for positioning at the designated angle. However, the depth error has the opposite

results. The manual surgery had more accurate and precise results than the robotic surgery. The depth error was the largest of all the errors in our results. The depth control of the disc was the most difficult osteotomy type performed in this study. In the future, we need an algorithm that can feedback the resistance of the robot while it performs osteotomy in order to achieve more accurate depth control.

Safety is one of the most important issues, and our robot has several integrated safety features. One of them is protection of the patient and the surgeon against a patient's unexpected movement. When the robot is touched by external force more than 15 N in the surgical field, it automatically stops moving, as it did during manual operation. As an amount of external force, we can modify the threshold of unpredicted external force. The ergonomic aspects of the robot guidance were assessed and confirmed under optimal conditions. The robot arm osteotomy was compact enough to allow two surgeons to operate comfortably. In the future, the robot will be able to play the role of one surgeon in the operating room.

Future research should be focused on the improvement of the real-time interaction between the end-effect of the robot and the target patient. More investigations are also needed to measure the dynamic data of ablated bone tissue, and for real-time monitoring and control of the depth of the disc or saw cut. This real-time interaction will add another important safety feature.

In this study, it was found that direct coordinate recognition by three points on the teeth using the robotic arm can be useful in autonomous robot surgery. However, further research should focus on how to track patient movement after

registration. We can track a designated point with a 3D camera or laser scanner and achieve the same effect as a navigation system with simpler equipment. Also, by using another robot arm connected to the patient's head for tracking, we can determine the movement of the patient's head position directly. This tracking method remains an additional challenge, and engineers and surgeons need to work together to overcome it.

5. Conclusion

An autonomous robot osteotomy scheme was developed, using the direct coordinate determination by three points on the teeth, and proved an accurate method for registration. The incisal edge or buccal pit of the teeth were more proper reference points than the fossa of the teeth. The measured RMS of the TRE increased when the target moved away from the reference points. Robotic surgery showed high accuracy and precision in positioning and reduced accuracy in controlling the depth of disc sawing. The robotic surgery showed high accuracy and precision in positioning and somewhat low accuracy in controlling the depth of the disc sawing. Comparing robotic and manual surgeries, the robotic surgery was superior in accuracy and precision in position, length and angle. However, the manual surgery had higher accuracy and precision in depth.

6. References

1. Moustris GP, Hiridis SC, Deliparaschos KM, Konstantinidis KM: Evolution of autnomous and semi-autnomous robotic surgical systems: a review of the literature. Int J Med Robot 7: 375, 2011.
2. Korb W, Marmulla R, Raczkowsky J, Mühling J, Hassfeld S: Robots in the operating theatre - Chances and challenges. Int J Oral Maxillofac Surg 33: 721, 2004.
3. Al-Rodhan NRF, Kelly PJ: Pioneers of stereotactic neurosurgery. Stereotact Funct Neurosurg 58: 60, 1992.
4. Kosugi Y, Watanabe E, Goto J, Watanabe T, Yoshimoto S, Takakura K, Ikebe J: An articulated neurosurgical navigation system using MRI and CT images. IEEE Trans Biomed Eng 35: 147, 1988.
5. Eggers G, Mühling J, Marmulla R: Image-to-patient registration techniques in head surgery. Int J Oral Maxillofac Surg 35: 1081, 2006.
6. Schneider J, Kalender W: Geometric accuracy in robot-assisted total hip replacement surgery. Comput Aided Surg 8: 135, 2003.
7. Sugano N: Computer-assisted orthopaedic surgery and robotic surgery in total hip arthroplasty. Clin Orthop Surg 5: 1, 2013.
8. Ballantyne GH: Robotic surgery, telerobotic surgery, telepresence, and telementoring. Surg Endosc Other Interv Tech 16: 1389, 2002.

9. Clavero J, Lundgren S: Ramus or Chin Grafts for Maxillary Sinus Inlay and Local Onlay Augmentation: Comparison of Donor Site Morbidity and Complications. Clin Implant Dent Relat Res 5: 154, 2003.
10. Kwon IJ, Lee BH, Eo MY, Kim SM, Lee JH, Lee SK: Pathologic mandibular fracture after biting crab shells following ramal bone graft. Dent Traumatol 32: 421, 2016.
11. Zhu JH, Deng J, Liu XJ, Wang J, Guo YX, Guo C Bin: Prospects of Robot-Assisted Mandibular Reconstruction with Fibula Flap: Comparison with a Computer-Assisted Navigation System and Freehand Technique. J Reconstr Microsurg 32: 661, 2016.
12. Gui H, Zhang S, Luan N, Lin Y, Shen SGF, Bautista JS: A novel system for navigation-and robot-assisted craniofacial surgery: Establishment of the principle prototype. J Craniofac Surg 26: e746, 2015.
13. Lee SJ, Woo SY, Huh KH, Lee SS, Heo MS, Choi SC, Han JJ, Yang HJ, Hwang SJ, Yi WJ: Virtual skeletal complex model- and landmark-guided orthognathic surgery system. J Cranio-Maxillofacial Surg 44: 557, 2016.
14. Augello M, Deibel W, Nuss K, Cattin P, Jürgens P: Comparative microstructural analysis of bone osteotomies after cutting by computer-assisted robot-guided laser osteotome and piezoelectric osteotome: an in vivo animal study. Lasers Med Sci: 1, 2018.
15. Suero EM, Westphal R, Zaremba D, Citak M, Hawi N, Citak M, Stuebig T, Krettek C, Liodakis E: Robotic guided waterjet cutting technique for high

tibial dome osteotomy: A pilot study. Int J Med Robot Comput Assist Surg 13: 1, 2017.

16. Baek KW, Deibel W, Marinov D, Griessen M, Bruno A, Zeilhofer HF, Cattin P, Juergens P: Clinical applicability of robot-guided contact-free laser osteotomy in cranio-maxillo-facial surgery: In-vitro simulation and in-vivo surgery in minipig mandibles. Br J Oral Maxillofac Surg 53: 976, 2015.

17. Kwoh YS, Hou J, Jonckheere EA, Hayati S: A robot with improved absolute positioning accuracy for CT guided stereotactic brain surgery. IEEE Trans Biomed Eng 35: 153, 1988.

18. Davies BL, Hibberd RD, Ng WS, Timoney AG, Wickham JEA: A surgeon robot for prostatectomies. In: Advanced Robotics, 1991.'Robots in Unstructured Environments', 91 ICAR., Fifth International Conference on., 1991:871–875.

19. Benabid AL, Cinquin P, Lavalle S, Bas JF Le, Demongeot J, Rougemont J De: Computer-driven robot for stereotactic surgery connected to CT scan and magnetic resonance imaging. Stereotact Funct Neurosurg 50: 153, 1987.

20. Yamauchi Y: A needle insertion Manipulator for X-ray CT image guided neurosurgery. Proc LST 5: 814, 1993.

21. Taylor RH, Mittelstadt BD, Paul HA, Hanson W, Kazanzides P, Zuhars JF, Williamson B, Musits BL, Glassman E, Bargar WL: An image-directed robotic system for precise orthopaedic surgery. IEEE Trans Robot Autom 10: 261, 1994.

22. Cleary K, Nguyen C: State of the art in surgical robotics: Clinical applications and technology challenges. Comput Aided Surg 6: 312, 2001.
23. Weihe S, Wehmöller M, Schliephake H, Haßfeld S, Tschakaloff A, Raczkowsky J, Eufinger H: Synthesis of CAD/CAM, robotics and biomaterial implant fabrication: Single-step reconstruction in computer aided frontotemporal bone resection. Int J Oral Maxillofac Surg 29: 384, 2000.
24. Majdani O, Rau TS, Baron S, Eilers H, Baier C, Heimann B, Ortmaier T, Bartling S, Lenarz T, Leinung M: A robot-guided minimally invasive approach for cochlear implant surgery: Preliminary results of a temporal bone study. Int J Comput Assist Radiol Surg 4: 475, 2009.
25. Zhu J-H, Wang J, Wang Y-G, Li M, Liu X-J, Guo C-B: Prospect of robotic assistance for fully automated brachytherapy seed placement into skull base: Experimental validation in phantom and cadaver. Radiother Oncol, 2017.
26. Ho AL, Muftuoglu Y, Pendharkar A V, Sussman ES, Porter BE, Halpern CH, Grant GA: Robot-guided pediatric stereoelectroencephalography: single-institution experience.: 1, 2018.
27. Zhou S, Zhang C, Li D: Approaches of robot-assisted neck dissection for head and neck cancer: A review. Oral Surg Oral Med Oral Pathol Oral Radiol 121: 353, 2016.

28. Shen Z, Li J, Chen W, Fan S: The Latest Advancements in Selective Neck Dissection for Early Stage Oral Squamous Cell Carcinoma. Curr Treat Options Oncol 18: 31, 2017.

29. Katz RD, Rosson GD, Taylor JA, Singh NK: Robotics in microsurgery: Use of a surgical robot to perform a free flap in a pig. Microsurgery 25: 566, 2005.

30. Zhu JH, Deng J, Liu XJ, Wang J, Guo YX, Guo C Bin: Prospects of Robot-Assisted Mandibular Reconstruction with Fibula Flap: Comparison with a Computer-Assisted Navigation System and Freehand Technique. J Reconstr Microsurg 32: 661, 2016.

31. Jung SW, Kim YK, Cha YH, Koh YW, Nam W: Robot-assisted submandibular gland excision via modified facelift incision. Maxillofac Plast Reconstr Surg 39: 25, 2017.

32. Chao AH, Weimer K, Raczkowsky J, Zhang Y, Kunze M, Cody D, Selber JC, Hanasono MM, Skoracki RJ: Pre-programmed robotic osteotomies for fibula free flap mandible reconstruction: A preclinical investigation. Microsurgery 36: 246, 2016.

33. Woo SY, Lee SJ, Yoo JY, Han JJ, Hwang SJ, Huh KH, Lee SS, Heo MS, Choi SC, Yi WJ: Autonomous bone reposition around anatomical landmark for robot-assisted orthognathic surgery. J Cranio-Maxillofacial Surg 45: 1980, 2017.

34. Zhou C, Zhu M, Shi Y, Lin L, Chai G, Zhang Y, Xie L: Robot-Assisted Surgery for Mandibular Angle Split Osteotomy Using Augmented Reality:

Preliminary Results on Clinical Animal Experiment. Aesthetic Plast Surg 41: 1228, 2017.

35. Klein M, Hein A, Lueth T, Bier J: Robot-assisted placement of craniofacial implants. Int J Oral Maxillofac Implants 18: 712, 2003.

36. Lueth TC, Hein A, Albrecht J, Demirtas M, Zachow S, Heissler E, Klein M, Menneking H, Hommel G, Bier J: A surgical robot system for maxillofacial surgery. In: Industrial Electronics Society, 1998. IECON'98. Proceedings of the 24th Annual Conference of the IEEE.Vol 4., 1998:2470–2475.

37. Peacock ZS, Aghaloo T, Bouloux GF, Cillo JE, Hale RG, Le AD, Lee JS, Kademani D: Proceedings from the 2013 American association of oral and maxillofacial surgeons research summit. J Oral Maxillofac Surg 72: 241, 2014.

38. Shoemake K: Euler angle conversion. Graph gems IV: 222, 1994.

39. C. Q, Z. C, S. F, Y. W, Y. S, C. P, C. W: An oral and maxillofacial navigation system for implant placement with automatic identification of fiducial points. Int J Comput Assist Radiol Surg, 2018.

40. Bettschart C, Kruse A, Matthews F, Zemann W, Obwegeser JA, Grätz KW, Lübbers HT: Point-to-point registration with mandibulo-maxillary splint in open and closed jaw position. Evaluation of registration accuracy for computer-aided surgery of the mandible. J Cranio-Maxillofacial Surg 40: 592, 2012.

41. Hoffmann J, Westendorff C, Leitner C, Bartz D, Reinert S: Validation of 3D-laser surface registration for image-guided cranio-maxillofacial surgery. J Cranio-Maxillofacial Surg 33: 13, 2005.

42. Pham AM, Rafii AA, Metzger MC, Jamali A, Strong BE: Computer modeling and intraoperative navigation in maxillofacial surgery. Otolaryngol Neck Surg 137: 624, 2007.

43. Besl PJ, McKay ND: Method for registration of 3-D shapes. In: Sensor Fusion IV: Control Paradigms and Data Structures.Vol 1611., 1992:586–607.

44. Kavanagh KT: Applications of image-directed robotics in otolaryngologic surgery. Laryngoscope 104: 283, 1994.

45. Yang G-Z, Cambias J, Cleary K, Daimler E, Drake J, Dupont PE, Hata N, Kazanzides P, Martel S, Patel R V., Santos VJ, Taylor RH: Medical robotics—Regulatory, ethical, and legal considerations for increasing levels of autonomy. Sci Robot 2: eaam8638, 2017.

Tables and Figures

Table 1. The absolute differences in x-, y-, and z-axes, and root mean square (RMS) between positions in planning and the intraoperative detection by the robot at three reference landmarks for the evaluation of fiducial localization error (FLE).

Landmarks	Δx (mm)	Δy (mm)	Δz (mm)	RMS (mm)
#1 first point	0.28 ± 0.20	0.27 ± 0.24	0.39 ± 0.17	0.62 ± 0.18
#2 second point	0.48 ± 0.32	0.32 ± 0.28	0.25 ± 0.19	0.70 ± 0.34
#3 third point	0.60 ± 0.19	0.75 ± 0.56	0.51 ± 0.22	1.21 ± 0.32
mean	0.45 ± 0.27	0.45 ± 0.44	0.38 ± 0.22	0.84 ± 0.38
p value	0.019	0.019	0.028	0.000
Post-hoc	#1-#3	#1-#3	#2-#3	#1-#3
($p < 0.05$)		#2-#3		#2-#3

Table 2. The absolute differences in x-, y-, and z-axes, and root mean square (RMS) between the values detected by the robot and the true values measured using cone beam computer tomography (CBCT) data at the sixteen landmarks for the evaluation of target registration error (TRE)

Landmarks	Δx (mm)	Δy (mm)	Δz (mm)	RMS (mm)
#1	1.17 ± 0.19	2.75 ± 0.68	0.53 ± 0.32	3.08 ± 0.57
#2	1.79 ± 0.40	1.20 ± 0.20	0.24 ± 0.14	2.20 ± 0.27
#3	0.48 ± 0.36	1.34 ± 0.11	1.11 ± 0.32	1.85 ± 0.21
#4	0.86 ± 0.39	1.60 ± 0.13	0.66 ± 0.21	1.98 ± 0.08
#5	0.28 ± 0.24	1.25 ± 0.08	0.73 ± 0.18	1.50 ± 0.13
#6	1.17 ± 0.10	0.92 ± 0.09	0.25 ± 0.14	1.51 ± 0.07
#7	0.36 ± 0.10	0.28 ± 0.17	0.52 ± 0.10	0.71 ± 0.09
#8	0.36 ± 0.13	0.11 ± 0.07	0.20 ± 0.14	0.45 ± 0.13
#9	2.28 ± 0.29	1.49 ± 0.24	1.49 ± 0.52	3.16 ± 0.24
#10	1.07 ± 0.24	1.62 ± 0.12	1.57 ± 0.13	2.51 ± 0.14
#11	0.37 ± 0.18	0.85 ± 0.36	0.50 ± 0.29	1.06 ± 0.46
#12	0.73 ± 0.26	1.25 ± 0.11	0.14 ± 0.18	1.48 ± 0.17
#13	0.83 ± 0.20	1.53 ± 0.40	0.27 ± 0.25	1.79 ± 0.42
#14	0.84 ± 0.09	1.72 ± 0.07	0.42 ± 0.04	1.96 ± 0.09
#15	0.43 ± 0.09	0.85 ± 0.31	0.19 ± 0.14	0.99 ± 0.30
#16	0.42 ± 0.10	0.57 ± 0.39	0.26 ± 0.17	0.80 ± 0.32
mean	0.84 ± 0.59	1.21 ± 0.67	0.57 ± 0.49	1.69 ± 0.82

Table 3. The absolute mean value and root mean square (RMS) of the target registration error (TRE) categorized by the right/left side and the mandible location

Landmarks	Δx (mm)	Δy (mm)	Δz (mm)	RMS (mm)
Right/Left				
Left side (n = 8 x 10 times)	0.81 ± 0.57	1.18 ± 0.82	0.53 ± 0.35	0.96 ± 0.47
Right side (n = 8 x 10 times)	0.87 ± 0.62	1.23 ± 0.48	0.61 ± 0.60	0.99±0.47
p value	0.506	0.625	0.329	0.662
Location				
#1 Anterior area (n = 4 x 10 times)	0.40 ± 0.11	0.45 ± 0.38	0.29 ± 0.19	0.58 ± 0.17
#2 Posterior area (n = 8 x 10 times)	0.69 ± 0.37	1.31 ± 0.35	0.51 ± 0.36	1.64 ± 0.38
#3 Coronoid/condyle (n = 4 x 10 times)	1.58 ± 0.57	1.76 ± 0.70	0.96 ± 0.67	2.12 ± 0.99
P value	0.000	0.000	0.000	0.000
Post-hoc ($p < 0.05$)	#1-#2 #1-#3 #2-#3	#1-#2 #1-#3	#1-#2 #1-#3 #2-#3	#1-#2 #1-#3 #2-#3

Table 4. The absolute mean value of osteotomy errors for position, angle, length, and depth in an RBG osteotomy model

Model RBG osteotomy (n=20)			Error (mean±SD)
Posterior cut	Position (mm)	Δy	0.61 ± 0.45
		Δz	0.59 ± 0.34
		RMS	0.85 ± 0.28
	Angle (Degree)		1.10 ± 1.24
	Length (mm)	Top	0.71 ± 0.27
		Bottom	0.93 ± 0.35
Anterior cut	Position (mm)	Δy	0.28 ± 0.17
		Δz	1.13 ± 0.80
		RMS	1.16 ± 0.55
	Angle (Degree)		1.54 ± 1.60
	Length (mm)	Top	0.74 ± 0.39
		Bottom	0.86 ± 0.33
Inferior disc cut	Position (mm)	Δy	0.54 ± 0.27
		Δz	1.00 ± 0.71
		RMS	1.14 ± 0.48
	Angle (Degree)	Anterior	1.00 ± 0.96
		Posterior	0.67 ± 0.74
	Depth (mm)	Anterior	0.75 ± 0.30
		middle	0.69 ± 0.42

		Posterior	0.76 ± 0.30
Inferior disc cut	Position (mm)	Δy	0.42 ± 0.33
		Δz	0.53 ± 0.43
		RMS	0.68 ± 0.36
	Angle (Degree)	Anterior	1.95 ± 1.61
		Posterior	1.32 ± 1.49
	Depth (mm)	Anterior	1.81 ± 0.68
		middle	1.71 ± 0.66
		Posterior	1.45 ± 0.82

RBG: ramal bone graft, SD: standard deviation, RMS: root mean square.

Table 5. Accuracy evaluation due to types of cut according to the absolute mean value on model RBG osteotomy

Cut	Error (mm, mean ± SD)
Posterior	0.77 ± 0.32
Anterior	0.82 ± 0.43
Inferior	0.76 ± 0.38
Superior	1.37 ± 0.83
p value	0.058

RBG: ramal bone graft, SD: standard deviation

Table 6. Accuracy evaluation due to the category of errors on model RBG osteotomy

Category		Error (mean ± SD)
Position (mm)	Δy	0.46 ± 0.34
	Δz	0.81 ± 0.65
	RMS	0.93 ± 0.45
Length (mm)		0.81 ± 0.34
Angle (Degree)		1.26 ± 1.35
Depth (mm)		1.19 ± 0.73
p value		0.000
Post-hoc ($p < 0.05$)		Position-Angle
		Position-Depth
		Length-Angle
		Length-Depth

SD: standard deviation

Table 7. The absolute mean values of osteotomy errors for position, angle, length and depth on mandible phantoms categorized by 6-mm disc and 20-mm discs in the robotic surgery group and the 6-mm disc and 20-mm disc in the manual surgery group

			Errors of Robot surgery			Errors of Hand surgery		
cut	category		6mm disc	20mm disc	*p* value	6mm disc	20mm disc	*p* value
Post.	Position (mm)	Δy	0.40 ± 0.09	0.55 ± 0.31	0.347	1.22 ± 0.55	0.61 ± 0.35	0.116
cut		Δz	0.51 ± 0.34	0.21 ± 0.13	0.251	1.50 ± 0.56	1.48 ± 0.67	0.834
		RMS	0.65 ± 0.17	0.59 ± 0.22	0.602	1.93 ± 0.37	1.60 ± 0.51	0.347
		variance	0.03	0.05		0.13	0.26	
	Angle (°)	mean±SD	0.72 ± 0.50	1.81 ± 1.29	0.754	6.13 ± 3.75	8.10 ± 2.67	0.057
		variance	0.25	1.67		14.07	7.11	
	Length (mm)	mean±SD	0.40 ± 0.14	0.33 ± 0.20	0.599	0.71 ± 0.26	0.91 ± 0.44	0.602
		variance	0.02	0.04		0.07	0.19	
	Position (mm)	Δy	0.96 ± 0.35	1.20 ± 0.31	0.175	1.48 ± 0.61	1.97 ± 0.98	0.347

Ant.		Δz	0.28 ± 0.14	0.45 ± 0.20	0.117	1.39 ± 0.70	1.59 ± 0.45	0.754
cut		RMS	1.00 ± 0.24	1.28 ± 0.22	0.251	2.03 ± 0.54	2.53 ± 0.42	0.347
		variance	0.06	0.05		0.29	0.17	
	Angle (°)	mean±SD	0.93 ± 0.62	1.17 ± 0.69	0.117	7.15 ± 3.15	1.74 ± 1.46	0.602
		variance	0.38	0.47		9.90	2.14	
	Length (mm)	mean±SD	0.40 ± 0.24	0.29 ± 0.13	0.347	0.39 ± 0.27	0.48 ± 0.24	0.463
		variance	0.06	0.02		0.07	0.06	
Inf.	Position (mm)	Δy	0.28 ± 0.27	0.36 ± 0.26	0.465	1.68 ± 0.48	2.00 ± 0.68	0.249
cut		Δz	0.23 ± 0.20	0.38 ± 0.19	0.347	1.56 ± 0.80	1.74 ± 0.68	0.602
		RMS	0.36 ± 0.32	0.52 ± 0.18	0.602	2.29 ± 0.51	2.65 ± 0.62	0.754
		variance	0.10	0.03		0.26	0.38	
	Angle (°)	mean±SD	0.29 ± 0.65	1.58 ± 0.96	0.753	7.58 ± 2.99	7.23 ± 3.55	0.754
		variance	0.42	0.92		8.94	12.63	
	Depth (mm)	mean±SD	0.36 ± 0.35	0.45 ± 0.30	0.530	0.32 ± 0.24	0.51 ± 0.33	0.251
		variance	0.12	0.09		0.06	0.11	

Sup.	Position (mm)	Δy	0.68 ± 0.29	0.26 ± 0.20	0.076	0.69 ± 0.21	1.01±0.56	0.602
cut		Δz	0.52 ± 0.65	0.46 ± 0.45	0.754	0.39 ± 0.30	0.40±0.18	0.917
		RMS	0.86 ± 0.45	0.53 ± 0.31	0.602	0.79 ± 0.20	1.09±0.41	0.465
		variance	0.20	0.09		0.04	0.16	
	Angle (°)	mean±SD	1.45 ± 1.08	1.30 ± 1.10	0.917	4.09 ± 2.80	5.29 ± 2.52	0.602
		variance	1.17	1.20		7.83	6.35	
	Depth (mm)	mean±SD	0.44 ± 0.21	1.13 ± 0.44	0.009	0.30 ± 0.25	0.46 ± 0.36	0.173
		variance	0.05	0.19		0.06	0.13	

RBG: ramal bone graft; SD: standard deviation; Post. cut: Posterior cut; Ant. cut: Anterior cut; Inf. cut: inferior cut; Sup. cut: Superior cut.

Table 8. Comparison of accuracy between robotic and manual surgeries for position, length, angle and depth errors

		Robot surgery	Hand surgery	P value
Position	Δy	0.59 ± 0.46	1.33 ± 0.78	0.000
	Δz	0.38 ± 0.35	1.25 ± 0.77	0.000
	RMS	0.70 ± 0.34	1.83 ± 0.65	0.000
	variance	0.11	0.43	0.000
Length	mean±SD	0.35 ± 0.19	0.62 ± 0.37	0.009
	variance	0.03	0.14	0.004
Angle	mean±SD	1.32 ± 0.96	5.96 ± 3.47	0.000
	variance	0.93	12.08	0.000
Depth	mean±SD	0.59 ± 0.46	0.40 ± 0.31	0.030
	variance	0.21	0.10	0.014

Figure legends

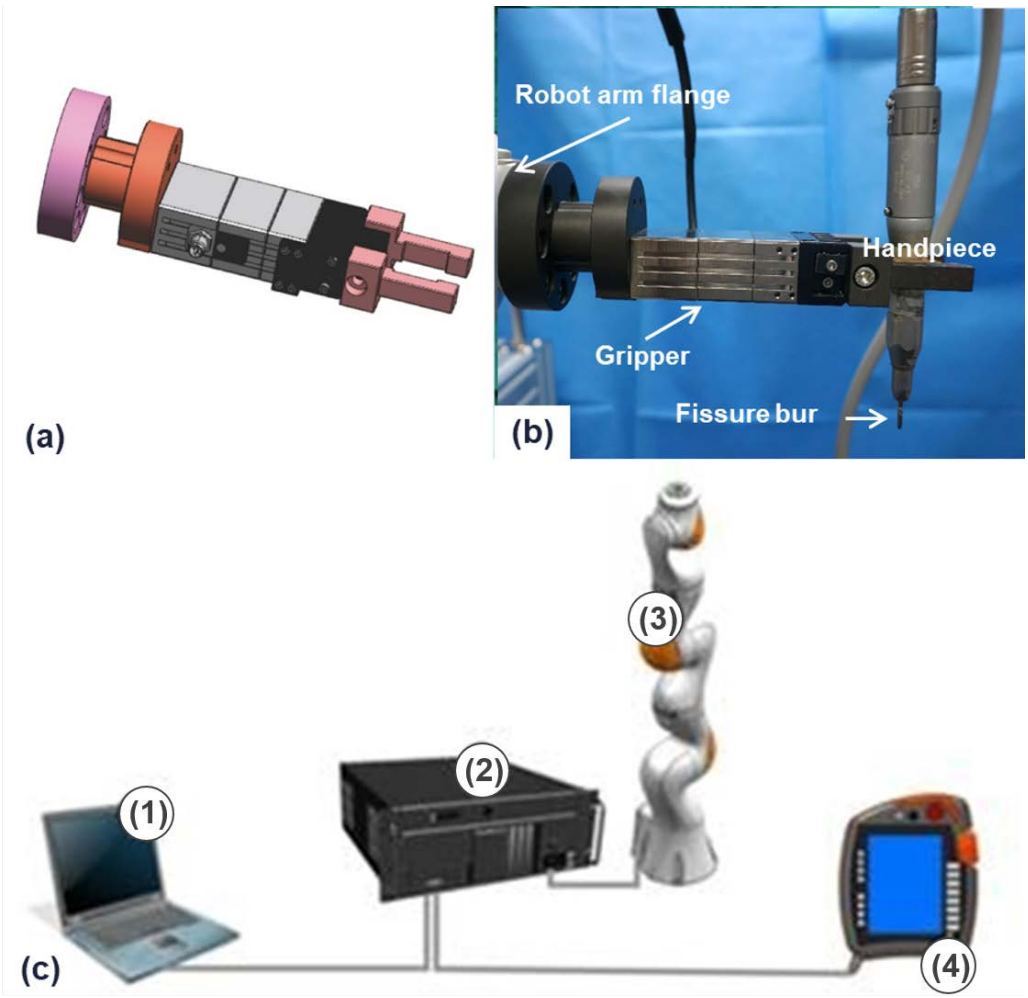

Figure 1. The design of electric gripper (a), the design of assembly tool for gripping a handpiece (b) and system setup of the robot-workbench notebook (1), robot controller (2), robot arm (3), and smartPAD® (4) (c)

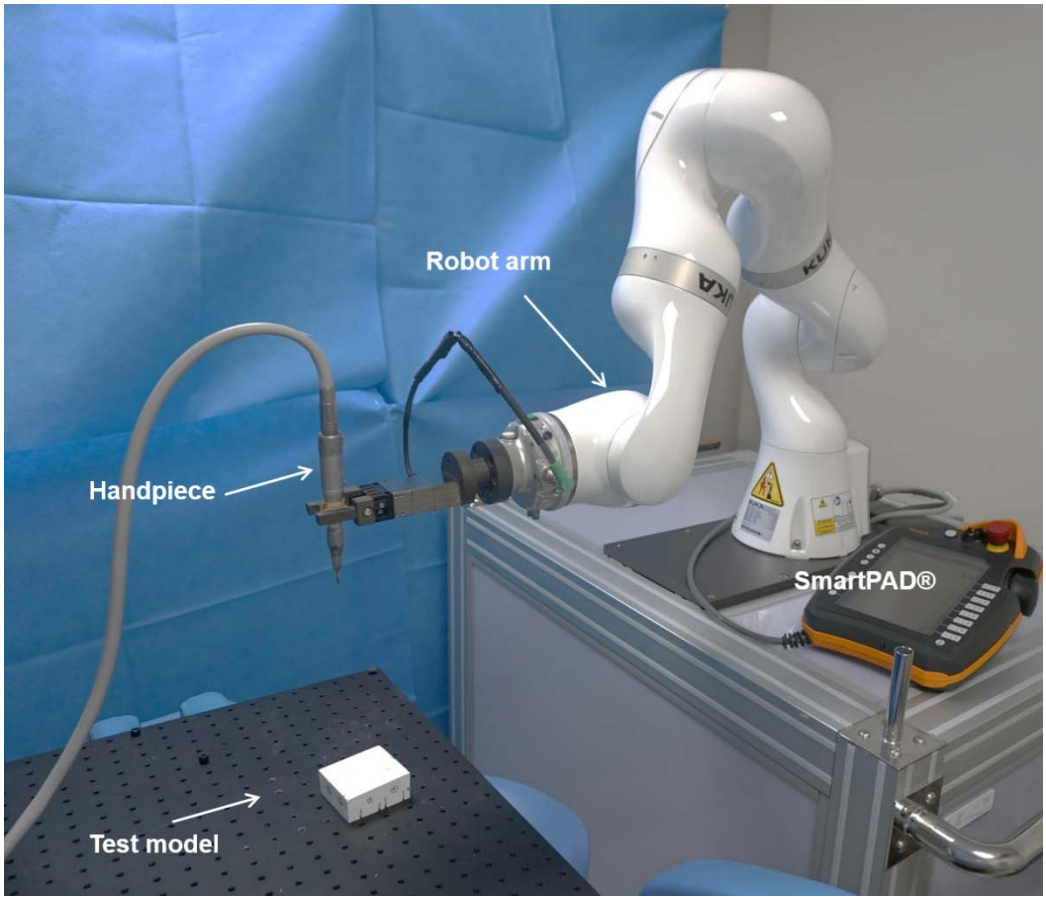

Figure 2. Overview of our autonomous robot osteotomy system.

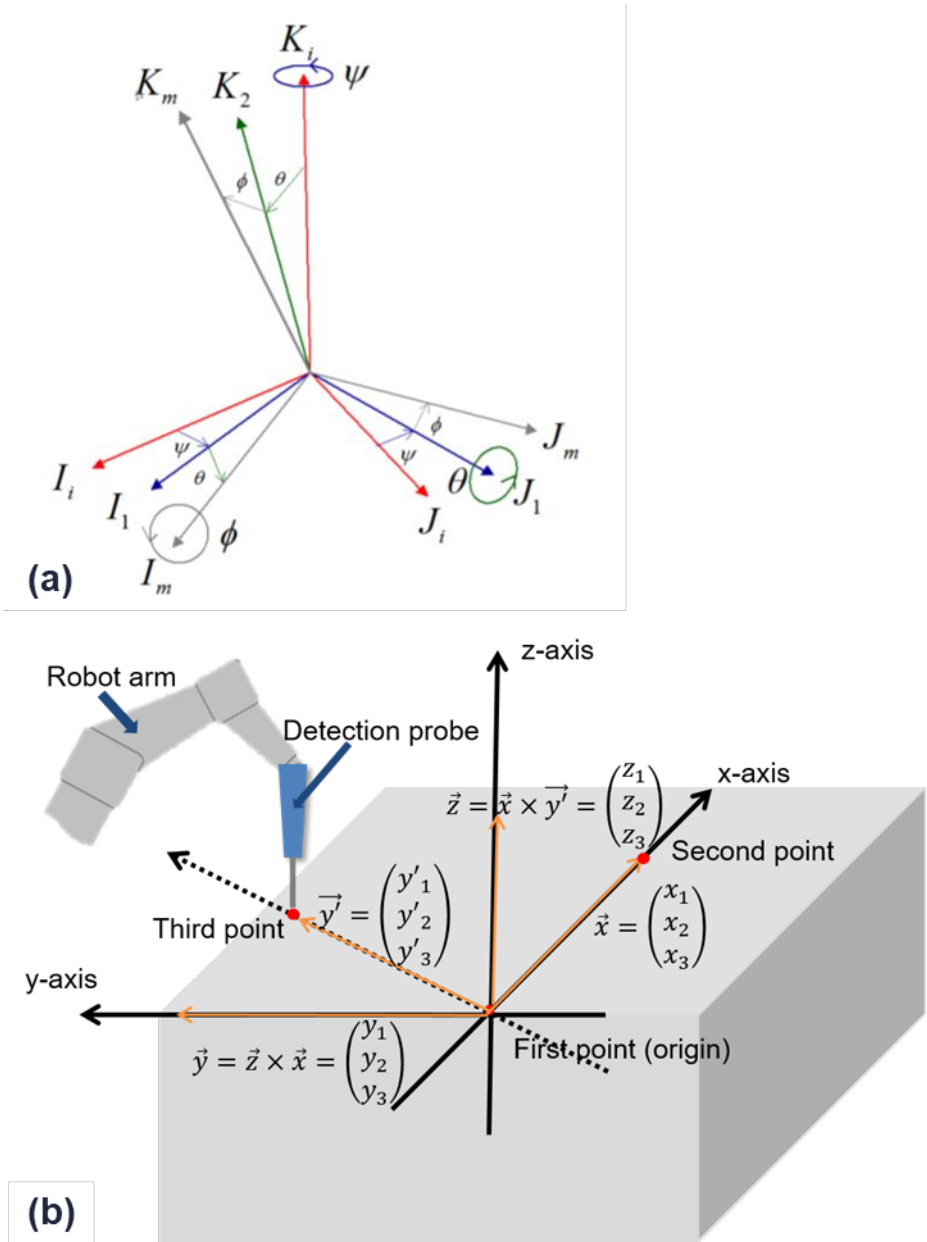

Figure 3. The 3D coordinate transformation between two coordinates by Euler angle conversion (a) and overview of the three-points coordinate determination using Euler angle conversion (b).

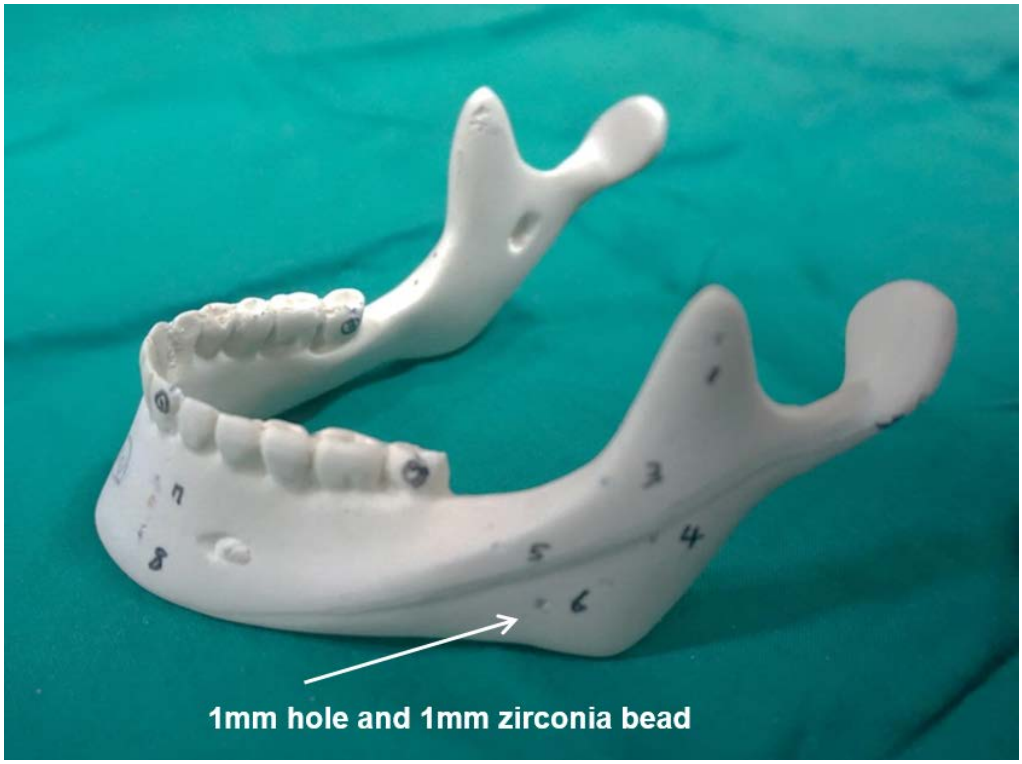

Figure 4. A prepared mandible model for testing the fiducial localization error and target registration error. A 1 mm diameter hole was made and a zirconia sphere bead with 1 mm diameter was put in the hole.

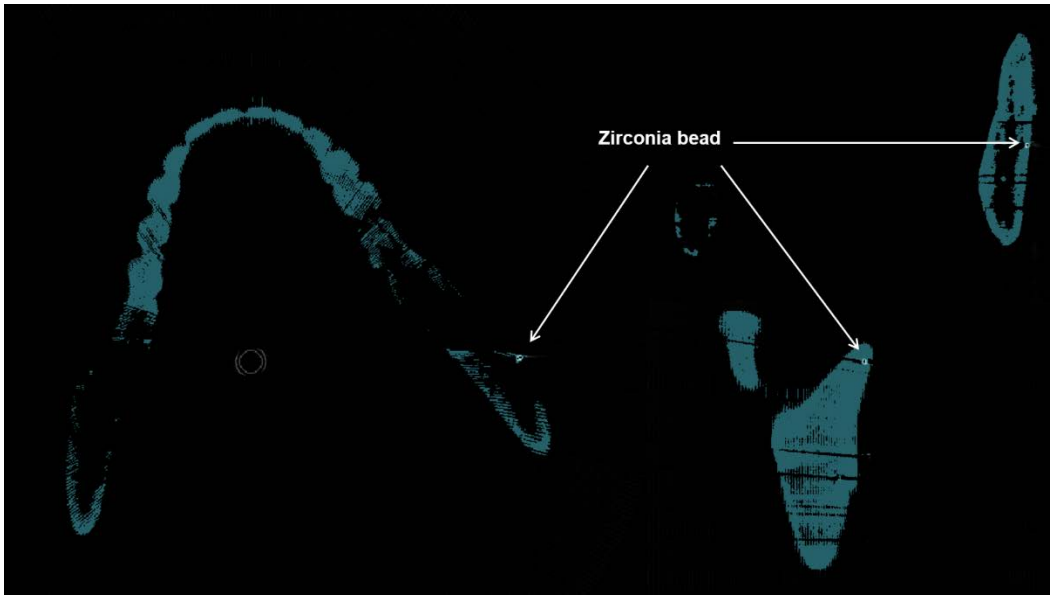

Figure 5. Scanned cone beam computer tomography image and landmarks which were made visible by zirconia beads.

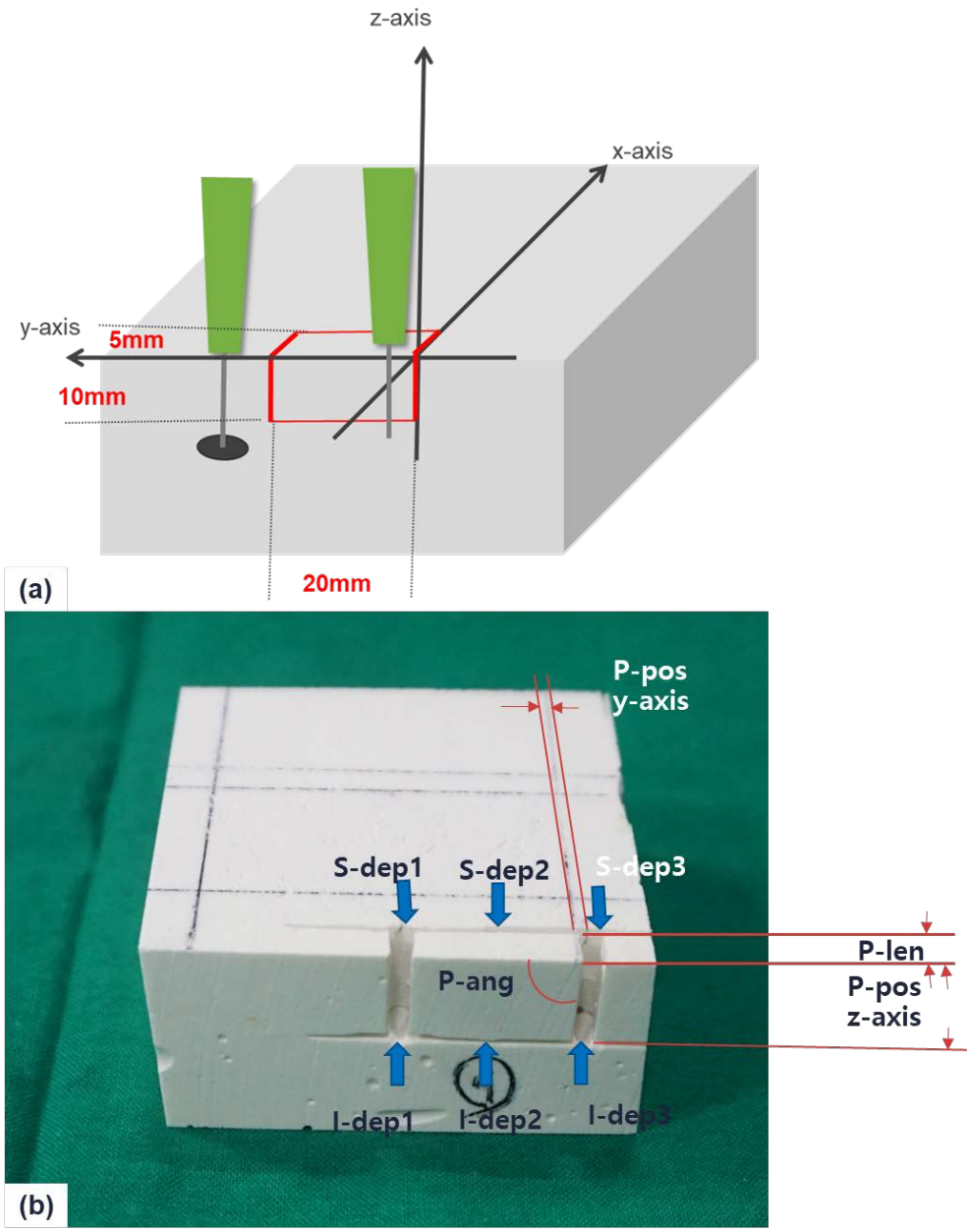

Figure 6. Design of model ramal bone graft osteotomy (a), measurements of model ramal bone graft osteotomy. P-pos: posterior position error, P-len: posterior length error, P-ang: posterior angle error, I-dep: inferior depth error, S-dep: superior depth error (b).

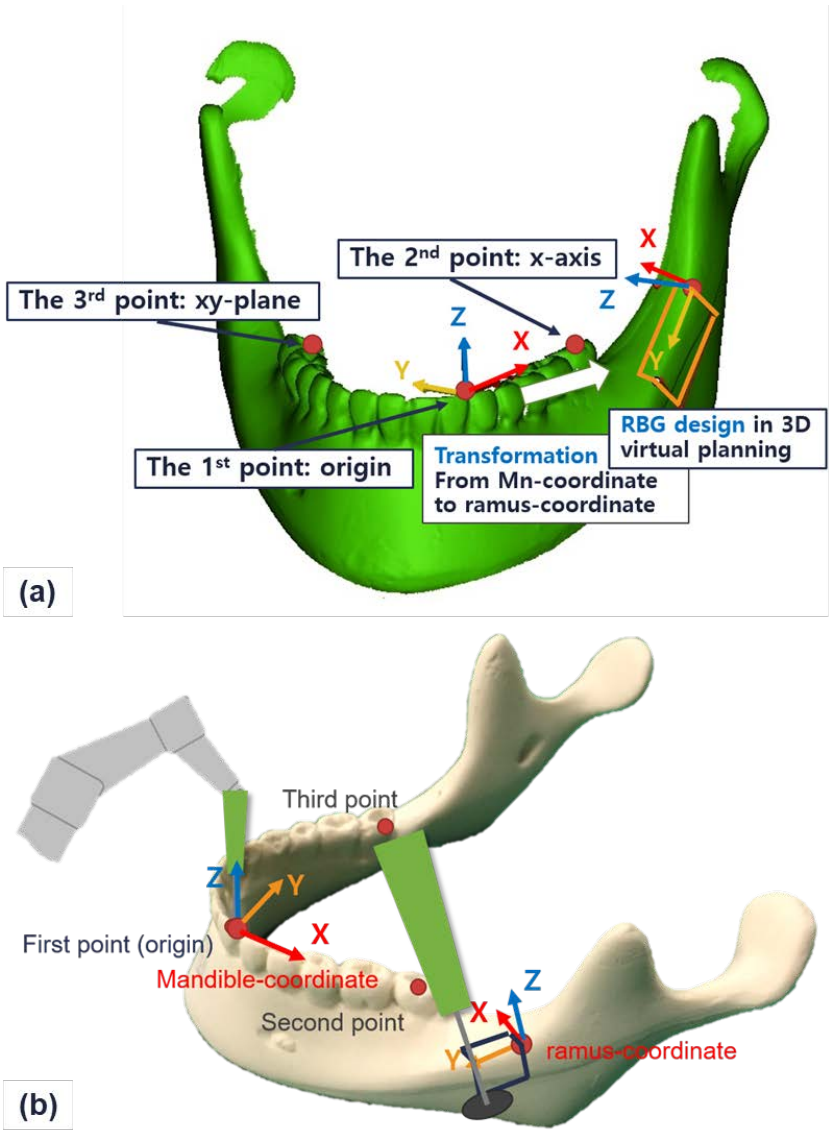

Figure 7. Schematic for the three-point coordinate determination and coordinate transform for the mandible phantom model. The ramal bone graft osteotomy was designed on the left ramus area (a). Schematics of the three-point coordinate determination and ramal bone graft osteotomy on the mandible phantom (b).

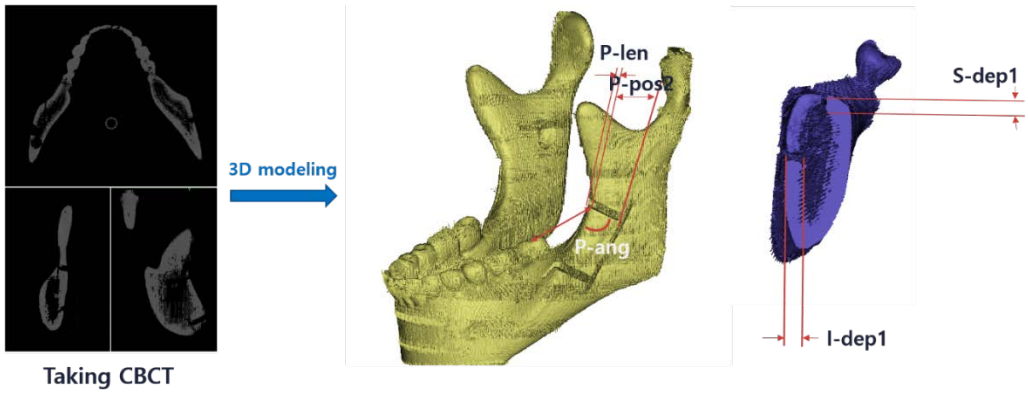

Figure 8. Accuracy evaluation of the mandible ramal bone graft osteotomy using cone beam computer tomography (CBCT) and 3D modeling with 3D software. P-pos: posterior position error, P-len: posterior length error, P-ang: posterior angle error, I-dep: inferior depth error

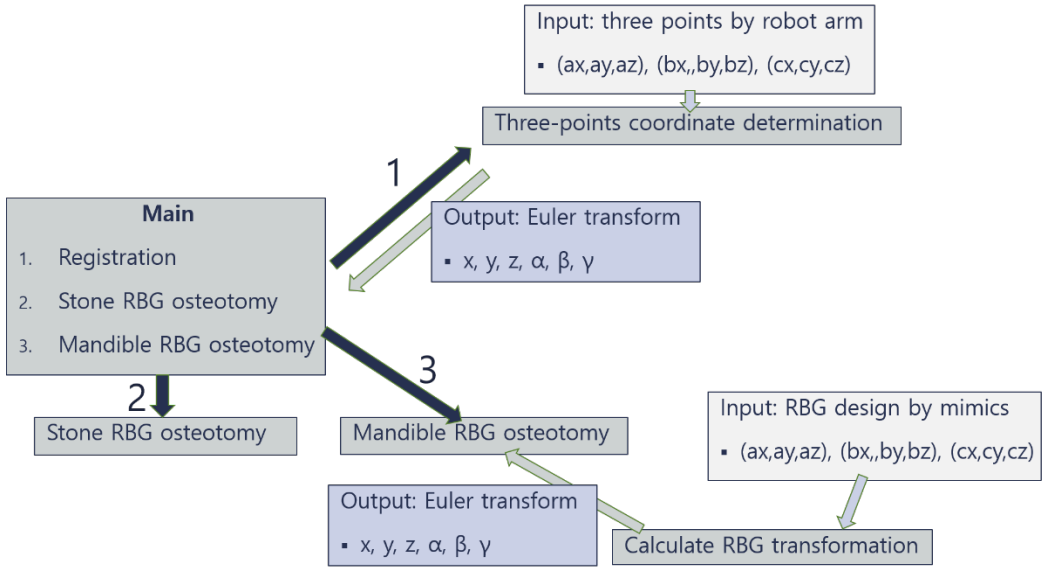

Figure 9. Work flow diagram for the autonomous robot osteotomy system. RBG: ramal bone graft

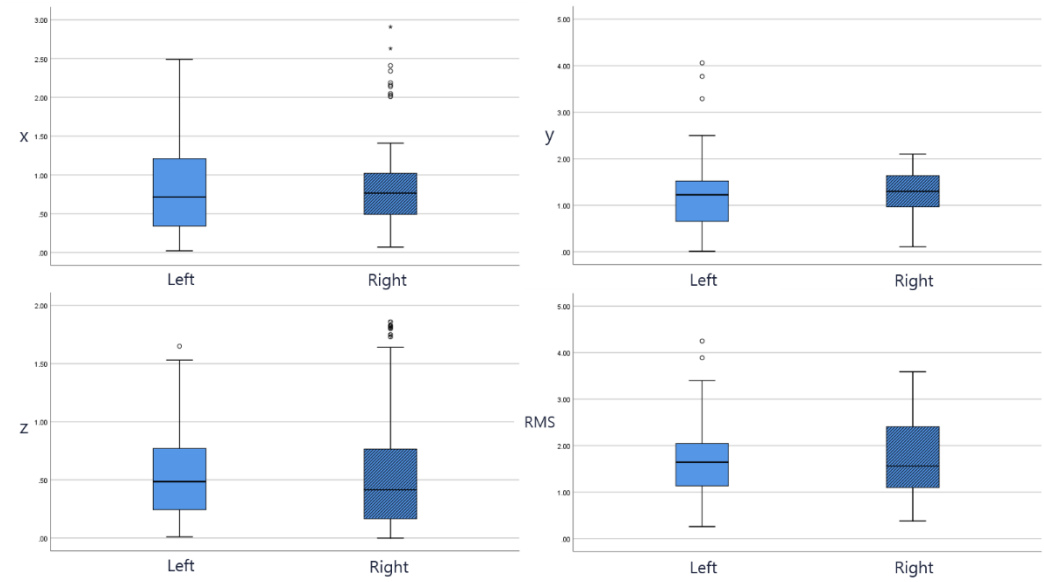

Figure 10. The absolute mean value (x-, y- and z-axes) and root mean square (RMS) of target registration error (TRE) categorized by right/left groups. There was no significant difference between the two groups.

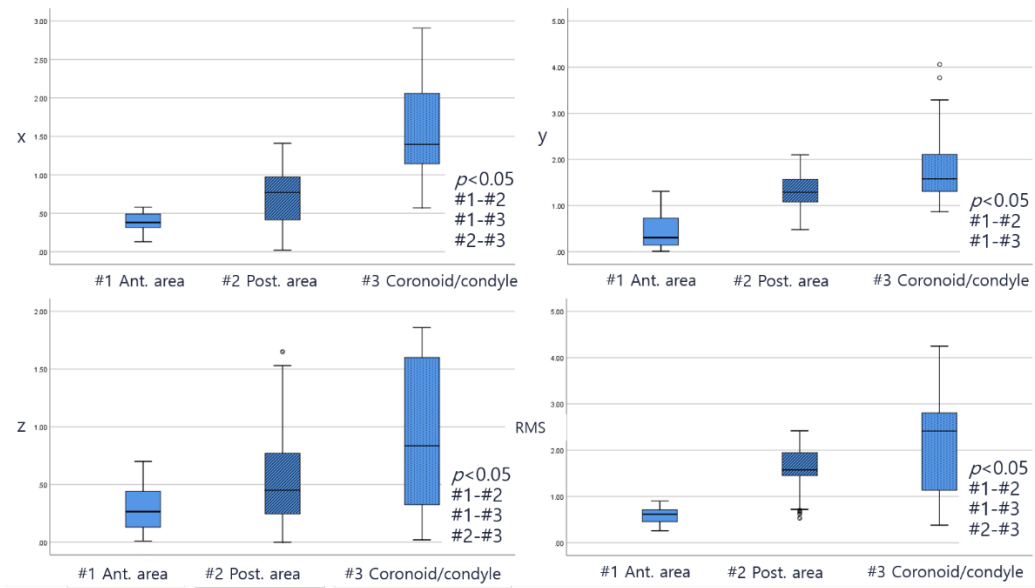

Figure 11. The absolute mean value (x-, y- and z-axes) and root mean square (RMS) of target registration error (TRE) categorized by the mandible location.

.

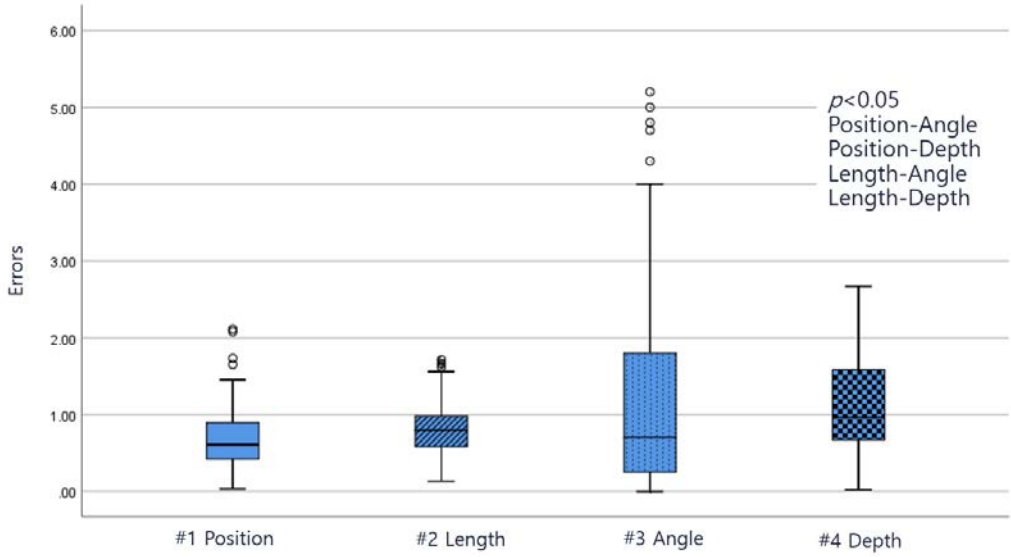

Figure 12. Accuracy evaluation by category of errors. Depth error was larger than angle error (marked as an asterisk, $p<0.05$).

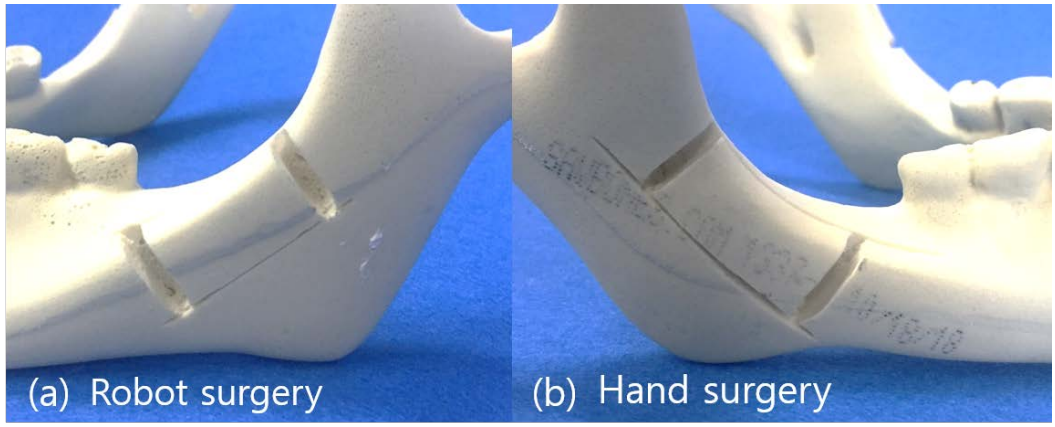

Figure 13. The results of the mandible ramal bone graft osteotomy using a robot (a) or freehand (b).

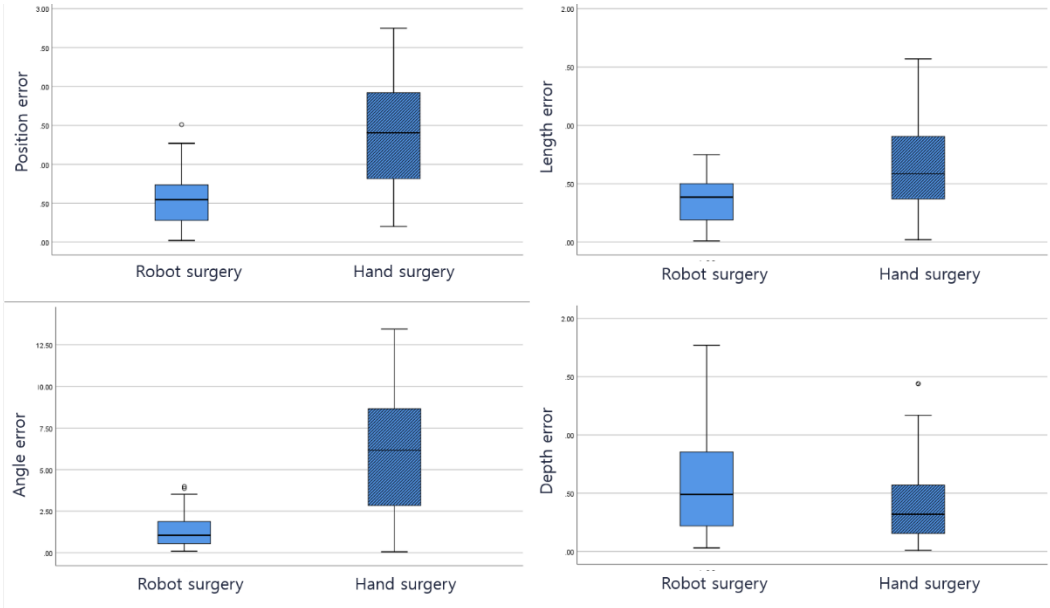

Figure 14. Mean and root mean square (RMS) errors (in mm) for the 6-mm disc and 20-mm disc for the robotic and manual surgeries: (a) and (b). Mean and RMS errors (in degrees): (c) and (d) due to types of cut. There were significant differences in all categories except the mean value of angle error (marked with an asterisk, $p<0.05$).

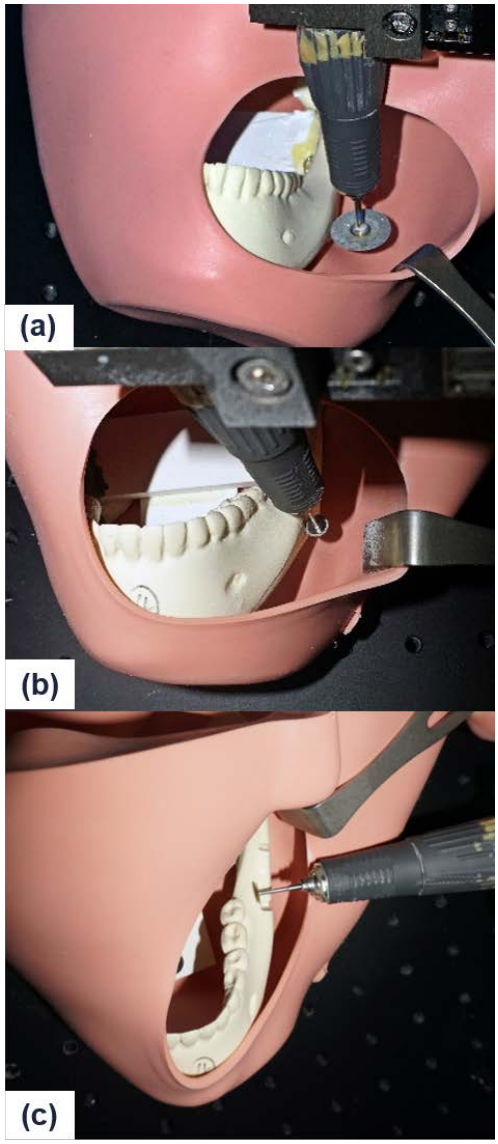

Figure 15. Test for the ease with which the posterior mandibular ramal area could be approached by the robot arm osteotomy through an intraoral approach in the dummy operating theater: inferior cut with 20 mm disc (a) and 6 mm disc (b), and superior cut with 6mm disc (c).

국문초록

로봇을 이용한 자율적 하악골채취 골절단술의 기초방법 개발과 그 정확도 평가

권 익 재

서울대학교 대학원

치의과학과 구강악안면외과학 전공

(지도교수 김 성 민)

1. 목 적

본 연구에서는 세 점 접촉을 통한 좌표 결정 방식을 통해 실제 모델의 좌표와 로봇이 가지고 있는 좌표를 정합하는 방식을 이용하여 자율 로봇을 이용한 하악골채취 골절단술의 기초방법을 개발하고자 한다. 개발된 정합 방법의 위치 추적 오류 (fiducial localization error)와 목표 정합 오류 (target registration error)를 측정하여 정합의 정확성을 평가하고자 한다. 또한 사전에 프로그래밍된 골절단을 직육면체 모델에 시행하고 위치, 길이, 각도, 깊이의 오류를 측정하여

정확성을 알아보고자 한다. 추가적으로 3 차원 가상수술을 통해 하악 상행지 골이식술(ramal bone graft)을 설계하고 하악 팬텀 모형에서 이에 맞게 자율 로봇이 골절단술을 수행하여 악골에서 있어서 로봇을 이용한 골절단술의 정확성을 평가해 보고 반대측은 대조군으로 외과의가 기존의 전통적인 방식으로 골절단술을 수행함으로써 양측을 비교하고자 한다.

2. 방 법

본 연구에서는 경량 로봇의 최종 작용체(end effector)에 전자 그리퍼(gripper)를 연결하고 이 그리퍼가 수술용 절삭기구나 디스크가 연결된 치과용 핸드피스를 잡고 골절단을 수행하도록 하였다. 실제 모델의 좌표와 로봇이 가지고 있는 좌표를 중첩하기 위해 세 점을 찍어 첫번째 점을 원점으로 하고, 두번째 점의 방향을 x 축으로, 그리고 세 번째 점이 결정하는 평면을 xy 평면으로 인식하도록 하였다. 첫번째 실험에서는 위치 추적 오류와 목표 정합 오류의 평가를 위해 하악골 모델에 치아의 기준 세 점과 하악골의 총 16 개의 목표 위치에 1mm 구멍을 뚫고 1mm 지름의 지르코니아 구를 적용하여 CBCT 상에서 잘 보일 수 있도록 하였다. 각 목표 위치에 10 번씩 반복하여 위치를 인식하여 오류를 계산하고 목표 정합 오류의 위치별 차이를 분석하였다. 두번째 실험에서는 총 20 개의 직육면체 석고 모델 (7cm x 7cm x 3cm)을 제작하였고 석고의 절단 크기는 하악 상행지 골채취을 위한 골절단 크기 (2cm x 1cm x 0.5cm)와 동일하게 설계하였다. 로봇팔을 이용하여 3 점 접촉을 하면 좌표값을 계산하여 미리

프로그래밍된 위치에서 골절단을 수행하였다. 로봇에 의해 수행된 석고 절단선은 위치, 길이 각도 및 깊이로 나누어 오류를 측정하였다. 세번째 실험에서는 하악 상행지 골채취를 위한 골절단 실험을 위해 총 16 개의 하악 팬텀 모형을 사용하였다. 팬텀 모형을 삼차원 스캐닝으로 삼차원 영상을 얻고 가상 수술을 시행하여 골절단 크기와 형태 그리고 그 위치에 대한 계획을 세웠다. 이 가상 수술 계획에 따라 로봇이 팬텀 모델에 골절단 수술을 하였다. 반대 측은 대조군으로 기존의 전통적인 방식으로 외과의가 수행하여 양측의 오차를 비교하였다. 절단선의 위치, 길이, 각도 및 깊이를 측정하여 각각의 정확도를 비교하였다. 위치 오류는 x 축으로는 로봇이 표면 접촉을 인식하고 골절단을 시행하기에 0 의 값으로 측정되었고 y 축과 z 축으로 나누어 측정되었으며 평균값과 제곱평균제곱근를 계산하였다.

3. 결 과

위치 추적 오류와 목표 정합 오류는 각각 0.49±0.22 mm 와 0.98±0.47 mm 로 측정되었으며 기준접에서 멀어질수록 목표 정합 오류는 더 큰 값을 보였다. 석고 모델 실험에서 절단선의 위치, 길이, 각도 및 깊이의 평균과 표준오차는 각각 0.93 ± 0.45 mm, 0.81 ± 0.34 mm, 1.26 ± 1.35˚, 1.19 ± 0.73 mm 이었다. 위치가 가장 정확한 값을 보였으며 길이 그리고 깊이 순으로 오차가 증가하였으며, 각도와 절단 깊이 제어가 가장 오차가 많은 술식이었다. 하악 팬텀 수술에서 로봇을 이용한 골절단의 위치, 길이, 각도 및 깊이 오차 값은 각각 0.70 ± 0.34

mm, 0.35 ± 0.19 mm, 1.32 ± 0.96°, 0.59 ± 0.46 mm 였으며 외과의의 골절단에서는 값이 각각 1.83 ± 0.65 mm, 0.62 ± 0.37 mm, 5.96 ± 3.47°, 0.40 ± 0.31 mm 였다. 위치, 길이, 각도 오차는 로봇이 더 작은 값을 보였고 깊이 오차는 외과의의 수술에서 더 작은 값을 보였다.

4. 결 론

본 연구에서는 하악 상행지 골채취를 위한 자율 로봇을 이용한 골절단 시스템을 개발하였고 위치추적오류와 목표정합오류 모두 우수한 값을 보였다. 석고 모형과 하악 팬텀 모향을 이용한 두가지 실험 모두에서 유용성과 향상된 정확성을 확인할 수 있었다. 세점 접촉 좌표 결정 시스템은 실제 모델의 좌표를 로봇의 좌표로 등록하는 데 유용한 시스템이었으며, 하악 상행지 골절단술에 대한 자율로봇 시스템의 정확도는 기존의 외과의가 직접 수행하는 방식보다 우수하였다.

주요어 : 자율 로봇, 세점 접촉 좌표 인식, 악골 절단술, 로봇 수술, 정확도

학 번 : 2014-30712